Carrier-density-dependent momentum shift of the coherent peak and the LO phonon mode in *p*-type high-T_c superconductors

S. Sugai, H. Suzuki, Y. Takayanagi, T. Hosokawa, and N. Hayamizu

Department of Physics, Faculty of Science, Nagoya University, Furo-cho, Chikusa-ku, Nagoya 464-8602, Japan

Systematic Raman scattering experiments were carried out in *p*-type superconductors YBCO, LSCO, Bi2212, and Bi2201. The superconducting coherent (pair-breaking) peak is anisotropic in *k* space not only in energy but also in existence itself. The position of the coherent peak in *k* space changes generally from $(\pi/2,\pi/2)$ to $(\pi,0)$, as carrier density increases, in correlation with the change of the low-energy electronic density of states. However, the change of the coherent peak in *k* space is more rapid than that of the electronic density of states, which suggests the existence of an additional pair-enhancing and pair-breaking mechanism. We found from two-phonon Raman scattering that the phonon mode with the strongest electron-phonon interactions changes from the breathing mode at (π,π) to the half-breathing mode at $(\pi,0)$ in good correlation with the change of the coherent peak. It suggests that electron-phonon interactions play an important role to generate the superconductivity in the limited region of *k* space, even if magnetic interactions are the main origin of the superconductivity.

I. INTRODUCTION

The pairing symmetry is one of the most intriguing problems for the mechanism of high-T_c superconductivity. Many experiments support $d(x^2-y^2)$ symmetry, which is expected from the magnetic interaction-mediated superconductivity mechanism. The direct observation of the *k*-dependent gap energy was obtained from angle-resolved photoemission spectroscopy (ARPES) in Bi2212 ($Bi_2Sr_2Ca_{1-x}Y_xCu_2O_{8+\delta}$).[1] Phase-sensitive experiments of π-superconducting quantum interference device,[2] tricrystal ring[3] in near-optimally-doped YBCO ($YBa_2Cu_3O_y$) support the $d(x^2-y^2)$ pairing. Raman scattering can also determine the pairing symmetry, because the B_{1g} and B_{2g} electronic Raman spectra are attributed to electronic excitations around $(\pi,0)$ and $(\pi/2,\pi/2)$, respectively.[4,5] The typical gap structure is composed of a valley around $\omega=0$ and a coherent peak (pair-breaking peak).[4–20] The gap energy along $(0,0)$-$(\pi,0)$ is the largest and that along $(0,0)$-(π,π) is zero for the $d(x^2-y^2)$ pairing. Therefore the B_{1g} coherent peak appears near the maximum pair-breaking energy $\omega=2\Delta$ (gap energy), while the B_{2g} coherent peak appears at low energy around the node direction. In optimally doped (OP) Bi2212, LSCO ($La_{2-x}Sr_xCuO_4$), and Tl2201 ($Ta_2Ba_2CuO_{6+\delta}$) both B_{1g} and B_{2g} coherent peaks were observed.[4,9–11,19,20] The results that the B_{1g} peak energies are larger than the B_{2g} peak energies are considered to support the $d(x^2-y^2)$ pairing.

The above ideal response for the $d(x^2-y^2)$ superconductivity is strongly modified in the underdoped (UD) region. The B_{2g} coherent peak is observed in the underdoped region of YBCO and LSCO, but the B_{1g} coherent peak is not observed.[12,15,17,18] In Bi2212 the small B_{1g} coherent peak coexists even at underdoping, although the intensity is small. It increases rapidly above the optimum doping, while the intensity of the B_{2g} coherent peak does not change so much from underdoping to overdoping.[10,16,19,20] It has been pointed out that the coherent peak symmetry is related to the low-

energy scattering intensity reflecting the electronic density of states near the Fermi energy (E_F).[12,15,17,18] However, the quantitative correlation is still controversial.

In order to clarify the correlation as common properties of high-T_c superconductors, systematic Raman-scattering experiments in many materials are requested. We carried out Raman-scattering experiments in YBCO, LSCO, Bi2212, and Bi2201 [$Bi_2Sr_{2-x}La_xCuO_{6+\delta}$ from the underdoped to the optimally doped region and $Bi_{1.74}Pb_{0.38}Sr_{1.88}CuO_{6+\delta}$ in the overdoped (OD) region] from the insulating phases to the overdoped phases. We found that the crossover of the coherent peak is not fully interpreted by the crossover of the low-energy density of states, because the change of the coherent peak is more rapid than the change of the low-energy scattering intensity. Furthermore, we found that the mode of the strongest two-phonon peak changes from Σ_1 mode at (π,π) to the Δ_1 mode at $(\pi,0)$ on the same longitudinal-optical (LO) phonon branch as carrier density increases. The good coincidence of the crossover carrier density and the crossover speed between the coherent peak and the phonon mode suggests that the electron-phonon interactions contribute to generate the superconducting states.

II. EXPERIMENT

Single crystals of YBCO were synthesized by a flux method utilizing Y_2O_3 crucibles. The obtained single crystals were sealed in quartz tubes with ceramics quenched from various temperatures and annealed at the same temperatures. The oxygen concentration was determined from the quenched temperature.[21] The amounts of oxygen and quenched temperatures are $y=6.2$ (930 °C), 6.33 (800 °C), 6.46 (700 °C), 6.54 (650 °C), 6.63 (600 °C), 6.68 (575 °C), 6.83 (500 °C), 6.91 (400 °C). Single crystals of LSCO, Bi2212, and Bi2201 were synthesized by a traveling-solvent-floating-zone method utilizing infrared radiation furnaces (Crystal system, FZ-T-4000) except for antiferromagnetic insulating (AFI) Bi2212 that was

TABLE I. Single crystals used in this experiment.

Compound	Doping	Holes/Cu	T_c	Initial composition	Annealing condition
$Bi_2Sr_2Ca_{0.5}Y_{0.5}Cu_2O_{8+\delta}$	AFI[a]	~0.01			5×10^{-5} mmHg at 550 °C
$Bi_2Sr_2Ca_{0.8}Y_{0.2}Cu_2O_{8+\delta}$	UD[b]	0.11	76 K	$Bi_{2.1}Sr_{1.9}Ca_{0.8}Y_{0.2}Cu_2O_{8+\delta}$	1×10^{-3} mmHg at 550 °C
$Bi_2Sr_2Ca_{0.8}Y_{0.2}Cu_2O_{8+\delta}$	UD	0.13	86 K	$Bi_{2.1}Sr_{1.9}Ca_{0.8}Y_{0.2}Cu_2O_{8+\delta}$	O_2 gas at 1 atm and 450 °C
$Bi_2Sr_2Ca_{0.9}Y_{0.1}Cu_2O_{8+\delta}$	OP[c]	0.16	93 K	$Bi_{2.1}Sr_{1.9}Ca_{0.9}Y_{0.1}Cu_2O_{8+\delta}$	O_2 gas at 1 atm and 450 °C
$Bi_2Sr_2CaCu_2O_{8+\delta}$	OD[d]	0.20	82 K	$Bi_{2.1}Sr_{1.8}CaCu_2O_{8+\delta}$	O_2 gas at 1 atm and 450 °C
$Bi_2SrLaCuO_{6+\delta}$	AFI	~0.02		$Bi_2SrLaCuO_{6+\delta}$	5×10^{-5} mmHg at 550 °C
$Bi_2Sr_{1.2}La_{0.8}CuO_{6+\delta}$	UD	0.067	9 K	$Bi_2Sr_{1.2}La_{0.8}CuO_{6+\delta}$	O_2 gas at 1 atm and 450 °C
$Bi_2Sr_{1.3}La_{0.7}CuO_{6+\delta}$	UD	0.093	23 K	$Bi_2Sr_{1.3}La_{0.7}CuO_{6+\delta}$	O_2 gas at 1 atm and 450 °C
$Bi_2Sr_{1.5}La_{0.5}CuO_{6+\delta}$	OP	0.16	32 K	$Bi_2Sr_{1.5}La_{0.5}CuO_{6+\delta}$	O_2 gas at 1 atm and 450 °C
$Bi_{1.74}Pb_{0.38}Sr_{1.88}CuO_{6+\delta}$	OD	0.23	21 K	$Bi_{1.74}Pb_{0.38}Sr_{1.88}CuO_{6+\delta}$	5×10^{-5} mmHg at 550 °C
$Bi_{1.74}Pb_{0.38}Sr_{1.88}CuO_{6+\delta}$	NSM[e]	0.28		$Bi_{1.74}Pb_{0.38}Sr_{1.88}CuO_{6+\delta}$	O_2 gas at 1 atm and 450 °C

[a]AFI: antiferromagnetic insulator.
[b]UD: underdoped superconductor.
[c]OP: optimally doped superconductor.
[d]OD: overdoped superconductor.
[e]NSM: no superconducting metal.

synthesized by a flux method. The La_2CuO_4 crystal was annealed in 1 mmHg oxygen gas at 900 °C for 12 h. The Néel temperature T_N is 293 K. The LSCO crystals of $x=0.2$ and 0.25 were annealed in oxygen gas under ambient pressure at 600 °C for 7 days. The annealing conditions for five Bi2212 crystals and six Bi2201 crystals are listed in Table I. The T_c was determined by electric resistivity. The widths of 10%–90% transitions are less than about 2 K indicating good crystals. The carrier density p in YBCO, Bi2212, and Bi2201was determined by the empirical equation[22]

$$T_c/T_{c,\max} = 1 - 82.6(p-0.16)^2, \qquad (2.1)$$

where $T_{c,\max}$ is the highest T_c in each series of the present experiment. In case of YBCO $y=6.46$, 6.54, 6.63, 6.68, 6.83, and 6.91 correspond to $p=0.062$, 0.081, 0.099, 0.11, 0.14, and 0.16, respectively. The carrier density p in LSCO is equal to x. The Raman spectra change according to the carrier density determined in this way.

Raman spectra were measured on fresh cleaved surfaces in a quasibackscattering configuration utilizing a 5145-Å Ar ion laser, a triple monochromator, and a charge-coupled device detector. The laser power was 5 or 10 mW for the measurement of low-energy spectra from 15 to 2000 cm^{-1} and 20 mW for the wide-energy spectra from 15 to 7000 cm^{-1}. The laser light was focused into an oval spot 50×500 μm^2 on the sample surface. The increase of temperature was less than about 2 K at 5 K for 10 mW, when it was estimated from the comparison of low-energy spectra at 5 K and 20 K with various excitation power 20, 10, 5, and 2 mW. The wide-energy spectra were obtained by shifting the central wave number of the spectrometer. The obtained spectra were corrected for the efficiency of the spectroscopic system utilizing a standard lamp to keep the constant response for the light power. Any artificial subtraction of the background was not done. Many spectra were measured twice in different crystals. Raman spectra were observed in four polarization configurations $(E_i, E_s)=(a,a)$, (a,b), (x,x), and (x,y),

where E_i and E_s are the polarizations of incident and scattered light, a and b are parallel to the Cu-O-Cu directions, and x and y are directions rotated by 45° from a and b axes in the ab plane. The Raman active symmetries are $A_{1g}+B_{1g}$, B_{2g}, $A_{1g}+B_{2g}$, B_{1g} for (a,a), (a,b), (x,x), and (x,y) polarization configurations, respectively. These spectra were measured on the same surface of a crystal. The (a,a) and (a,b) spectra were measured on the exactly same position. Similarly the (x,x) and (x,y) spectra were measured on the exactly same position.

Raman spectra can be presented in two kinds of forms: one is the originally observed spectra and the other is the Raman susceptibility χ which is obtained by dividing the original spectra by $n(\omega,T)+1$, where $n(\omega,T)$ is the Bose-Einstein statistical factor. For usual electronic excitations the temperature dependence at low energies is smaller in χ than in the original spectra, but in the marginal Fermi liquid[23] it is smaller in the original spectra. In the marginal Fermi liquid χ is approximately proportional to ω/T at $0<\hbar\omega<k_BT$ and constant above it. This temperature dependence makes the original spectra nearly independent of temperature. Electronic excitations in high-T_c superconductors show the marginal Fermi-liquid behavior in the large area of the momentum and carrier-density space.[24,25] In many cases the original Raman spectra are less temperature-dependent than χ at low energies in the normal phase. Another reason that we prefer the original spectra is that what we want to see is the electronic density of states near E_F. The intensity in χ always approaches zero below k_BT as the energy goes to zero, even if the electronic density of states is constant near E_F. It makes difficult to observe the low-energy excitations. On the other hand, the original spectra have no such property and make it easy to estimate the density of states near E_F. Therefore we present the original spectra in the following. The gap energies determined from both methods are almost the same, because the gap energies are larger than k_BT_c.
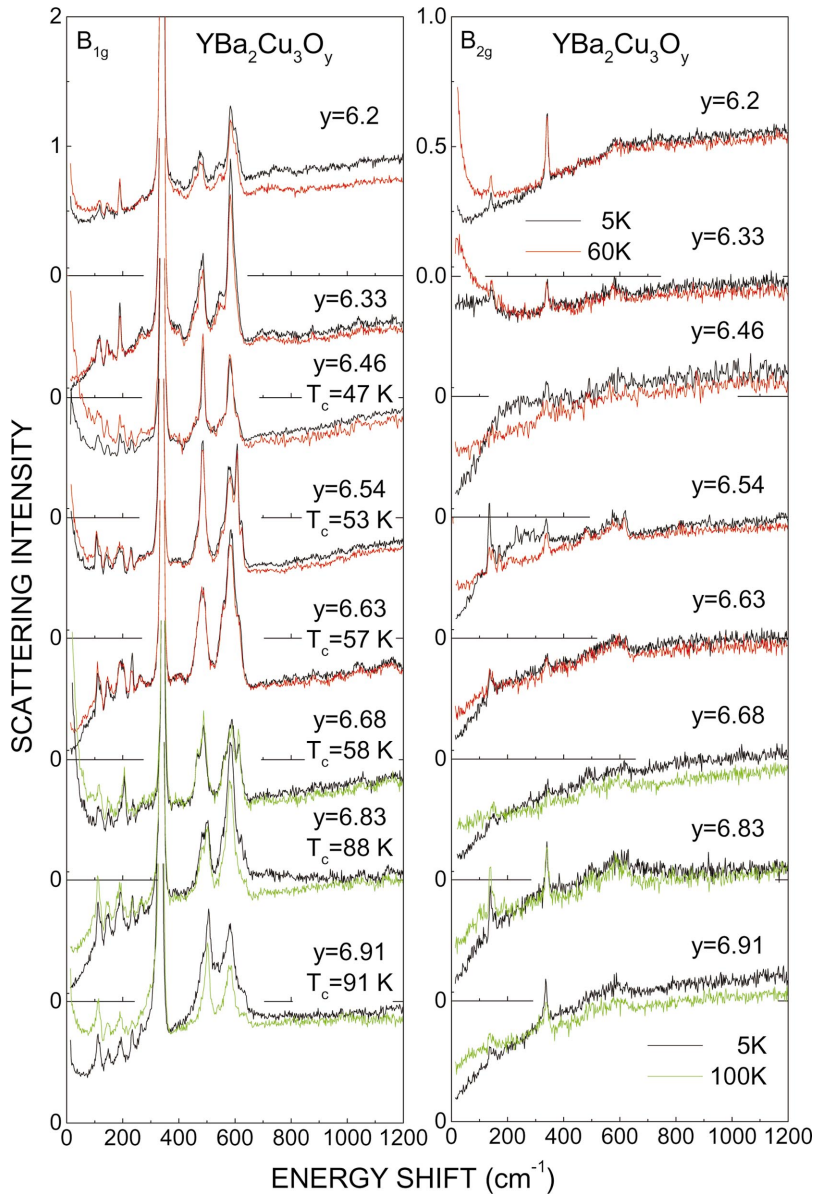
FIG. 1. (Color) B_{1g} and B_{2g} Raman spectra in YBCO at 5 K and just above T_c (60 K for $y \leqslant 6.63$ and 100 K for $y \geqslant 6.68$).

Infrared-ultraviolet reflection spectra were measured by a Fourier-transform infrared spectrometer (Bomem DA8) and a grating spectrometer.

III. SUPERCONDUCTING COHERENT PEAK, LOW-ENERGY SCATTERING INTENSITY, AND THE TWO-MAGNON PEAK

Raman spectra of YBCO contain extrinsic phonon peaks relating to chains in the reconstructed surface layer on the cleaved surface.[26,27] Those peaks can be bleached by the exposure of laser light at 20 K. Raman spectra were measured on the warming process after almost complete bleaching, but above 200 K those peaks appear again. Figure 1 shows the B_{1g} and B_{2g} Raman spectra in YBCO at the superconducting states (5 K) and the normal states (60 K for $y \leqslant 6.63$ and 100 K for $y \geqslant 6.68$). In the B_{2g} spectra the typical gap structure is observed at $y = 6.46$ and 6.54. The scattering intensity below 120 cm^{-1} at 5 K is smaller than that at 60 K and the inten-

sity around 250 cm^{-1} at 5 K is larger than that at 60 K. The increase of the scattering intensity around 250 cm^{-1} is due to the formation of the superconducting coherent peak. In the B_{1g} spectra the typical gap structure is observed at $y = 6.83$ and 6.91. The intensity below 360 cm^{-1} at 5 K is smaller than that at 100 K and the intensity around 600 cm^{-1} at 5 K is larger than that at 100 K by the formation of the coherent peak. The coherent peak was not observed above T_c.

In order to show clearly the change of electronic scattering induced by the superconducting transition, the differential spectra between the superconducting states and the normal states are shown in Fig. 2. The phonon structure is not completely subtracted for large peaks at 334, 506, and 582 cm^{-1} ($y = 6.91$) in the B_{1g} spectra. As carrier density increases, the coherent peak appears at 228 cm^{-1} in the B_{2g} spectra at $y = 6.46$ and the intensity increases at $y = 6.54$, but the coherent peak is not observed in the B_{1g} spectra in these carrier densities. The coherent peak decreases in the B_{2g} spectra at $y = 6.63$. In place of this decrease a coherent peak
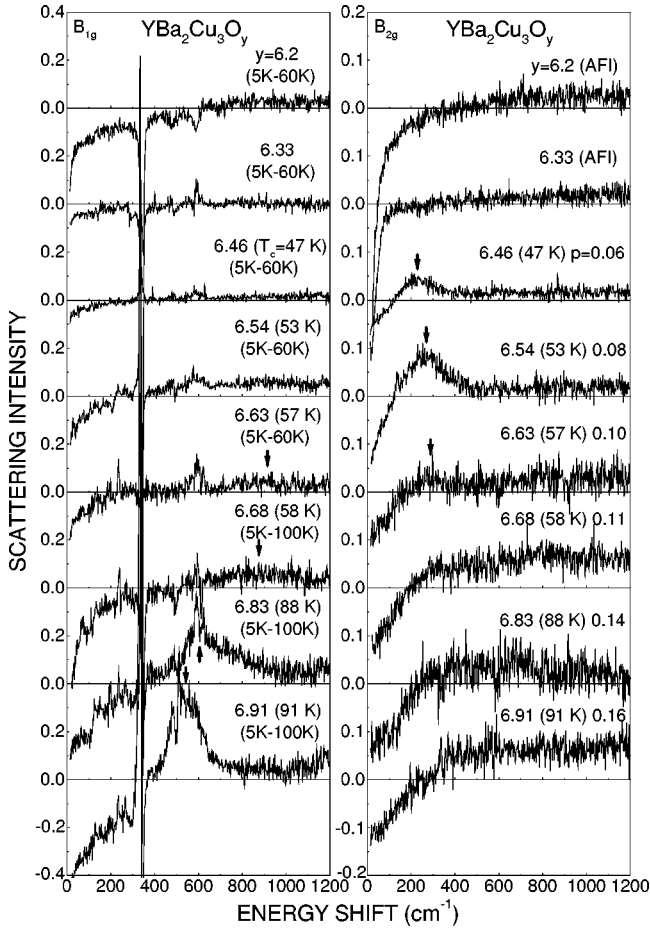
FIG. 2. Differential Raman spectra between 5 K and just above T_c (60 K for $y \leqslant 6.63$ and 100 K for $y \geqslant 6.68$).

appears at 914 cm^{-1} in the B_{1g} spectra. The B_{1g} coherent peak increases at $y = 6.83$ and 6.91, but the coherent peak is not observed in the B_{2g} spectra. The symmetry of the coherent peak clearly changes from B_{2g} to B_{1g} at $y = 6.63$ ($p = 0.99$). The coherent peak is small in both B_{2g} and B_{1g} at the crossover region $y = 6.63$ and 6.68 in the 60 K phase.

This symmetry crossover of the coherent peak is commonly observed in high-T_c superconductors. Figure 3 shows the B_{1g} and B_{2g} Raman spectra of LSCO in the superconducting states (5 K) and the normal states (40 K). Figure 4 shows the differential spectra between 5 K and 40 K. The coherent peak is observed in the B_{2g} spectra at the underdoped and optimally-doped region, $0.08 \leqslant x \leqslant 0.15$, while in the B_{1g} spectra at the optimally-doped and overdoped region, $0.15 \leqslant x \leqslant 0.22$. At $x = 0.115$ the B_{2g} coherent peak height is smaller than both sides. This is related to the "(1/8)-problem" that the T_c decreases by the formation of the quasistatic spin-charge stripe structure near $p = 1/8$.[28–30] The B_{2g} coherent peak energy increases gradually as carrier density increases. The energy of the B_{1g} coherent peak decreases monotonically from $x = 0.15$ to 0.22.

The carrier-density dependence of the low-energy scattering intensity is most clearly observed in LSCO. The B_{2g} intensity at low energies (for example, at 100 cm^{-1}) in the normal phase (at 40 K) decreases monotonically in the me-

tallic phase from $x = 0.06$ to 0.25. On the other hand, the B_{1g} low-energy intensity increases with the increase of carrier density. These changes are qualitatively consistent with the reported results in LSCO (Refs. 12,17,31,32) and Bi2212.[19,20,33] The low-energy intensity is proportional to the density of states near E_F. The opposite carrier-density dependence between B_{2g} and B_{1g} suggests that doped carriers enter mainly near $(\pi/2, \pi/2)$ at underdoping and near $(\pi, 0)$ at overdoping.

Figure 5 shows the B_{1g} and B_{2g} spectra of Bi2212 in the superconducting states (5 K) and in the normal states (100 K). Figure 6 shows the differential spectra between 5 K and 100 K. The coherent peak is observed from the underdoped region to the overdoped region in the B_{2g} spectra. On the other hand, the coherent peak is very small in the underdoped region in the B_{1g} spectra. It increases rapidly at the optimum doping and further increases as the carrier density increases.

Figure 7 shows the B_{1g} and B_{2g} spectra of Bi2201 in the superconducting states (5 K) and in the normal states (40 K). Figure 8 shows the differential spectra between 5 K and 40 K. The spectra of the nonsuperconducting metallic phase $Bi_{1.74}Pb_{0.38}Sr_{1.88}CuO_{6+\delta}$ were taken at 5 K and 100 K. The coherent peak is observed from the underdoped to the optimally-doped region in the B_{2g} spectra, while the very small coherent peak increases rapidly from the optimally-doped to the overdoped region in the B_{1g} spectra.

The B_{1g} coherent peak energy, which is considered as the superconducting gap energy 2Δ, is proportional to the exchange interaction energy determined from the B_{1g} two-magnon peak energy. Figure 9 shows the carrier-density dependence of the B_{1g} two-magnon spectra in YBCO, LSCO, Bi2212, and Bi2201 at 300 K. The two-magnon peak energy decreases, as carrier density increases, in agreement with other experiments.[17,19,32,34,35] The peak energies are almost the same in the insulating AF phase, but the decreasing rates are different. The decrease is the fastest in Bi2201 and the slowest in YBCO.

The difference between B_{1g} and B_{2g} symmetries is summarized as a function of carrier density in Fig. 10. Figure 10(a) shows the energy of the coherent peak. Figure 10(b) shows the height of the coherent peak measured from the level continued from 600–1200 cm^{-1} in the differential spectra. Figure 10(c) shows the relative height between the B_{1g} and B_{2g} coherent peaks. Figure 10(d) shows the low-energy scattering intensity at 100 cm^{-1}. Figure 10(e) shows T_c of the same crystal or a crystal in the same batch. The effective exchange interaction energy J^* obtained from the two-magnon peak energy $\omega_{2\text{-magnon}}$ by $J^* = \frac{1}{3}\omega_{2\text{-magnon}}$ is also shown in Fig. 10(a).

In YBCO the energy of the B_{2g} coherent peak at $y \leqslant 6.68$ ($p \leqslant 0.11$) is much lower than J^*, but the energy of the B_{1g} coherent peak at $y \geqslant 6.63$ ($p \geqslant 0.1$) is higher than J^*. In LSCO the B_{2g} ($x \leqslant 0.15$) and the B_{1g} ($x \geqslant 0.15$) coherent peak energies are lower than J^*. The B_{1g} coherent peak energy is proportional to J^*. In Bi2212 the B_{2g} coherent peak energy is much lower than J^* at $p = 0.11$. It increases to near J^* at $p = 0.16$ and follows the decreasing J^* in the
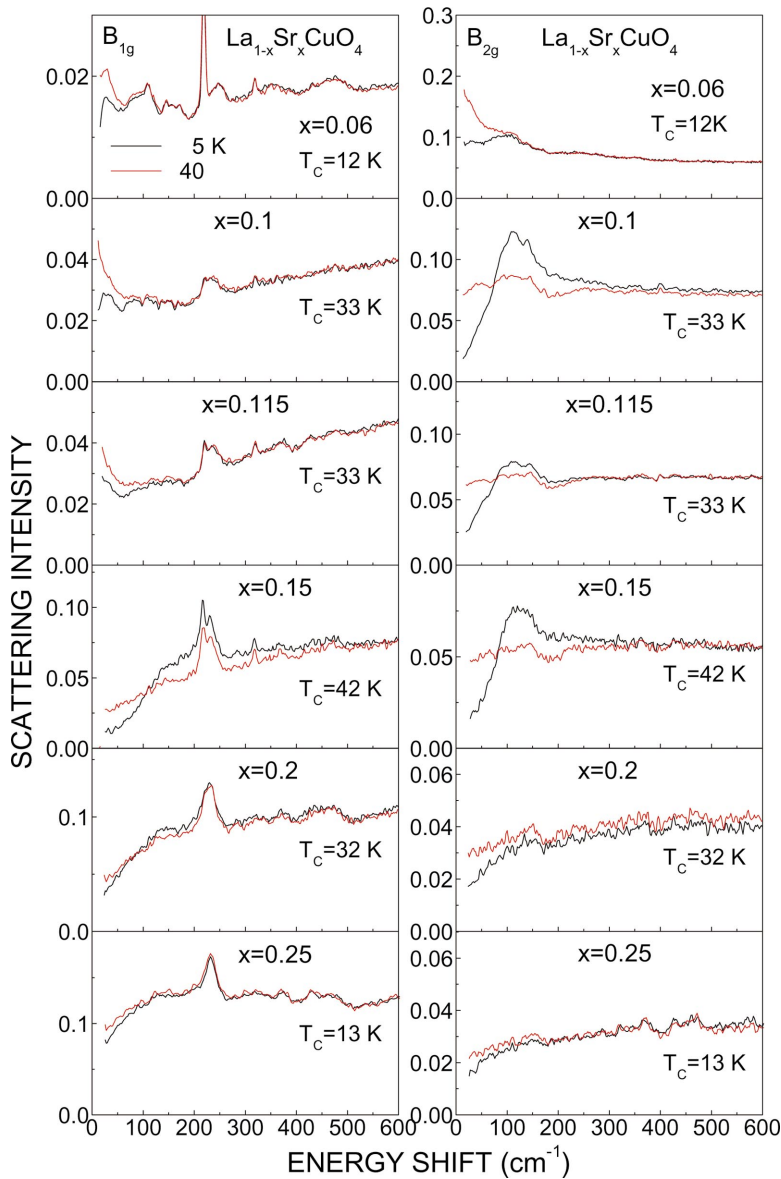
FIG. 3. (Color) B_{1g} and B_{2g} Raman spectra in LSCO at 5 K and 40 K.

overdoped region. The B_{1g} coherent peak energy is almost the same as J^* from the underdoped region to the overdoped region. The B_{2g} coherent peak height is larger than the B_{1g} peak height in the underdoped region. The relative height exchanges near optimum doping as shown in Fig. 10(c). In Bi2201 the B_{2g} coherent peak is observed only at the underdoped and optimally-doped region and the energy is lower than J^*. The height of the B_{1g} coherent peak is large from the optimally doped region to the overdoped region and the energy is almost the same as J^*.

Figure 10(d) shows the low-energy (100 cm^{-1}) electronic scattering intensity at 300 K and just above T_c (60 K for y ⩽6.63 and 100 K for y⩾6.68 in YBCO, 40 K in LSCO, 100 K in Bi2212, and 40 K in Bi2201). The typical carrier density dependence is observed in LSCO. The B_{2g} scattering intensity increases rapidly from AFI to the insulator-metal transition point and decreases gradually as carrier density increases, while the B_{1g} scattering intensity increases with the increase of carrier density. The crossover of the intensity

occurs near the optimum doping. It indicates that the carriers enter at $(\pi/2,\pi/2)$ in k space at low carrier density and move to $(\pi,0)$ as carrier density increases. The same carrier-density dependence is commonly observed in YBCO, Bi2212, and Bi2201. In YBCO the increase of the B_{1g} intensity from 100 K to 300 K is caused by the increase of extrinsic phonon scattering in the reconstructed surface layer on the cleaved surface. Theoretical models were proposed for the small density of states at $(\pi,0)$ and the large density of states at $(\pi/2,\pi/2)$ in the underdoped region. They are (1) interactions with the magnetic collective mode at (π,π) called as the "hot spots and cold spots" model,[36] (2) the instability of the Fermi liquid in strong-coupling umklapp scattering processes,[37] and (3) effects of second and third neighbor hopping terms.[38]

ARPES showed that the pseudogap starts to open at $(\pi,0)$ and extends to $(\pi/2,\pi/2)$ in underdoped Bi2212, as temperature decreases from the spin gap temperature (T_{SG}) to T_c.[39] In the Raman spectra the decrease of intensity from
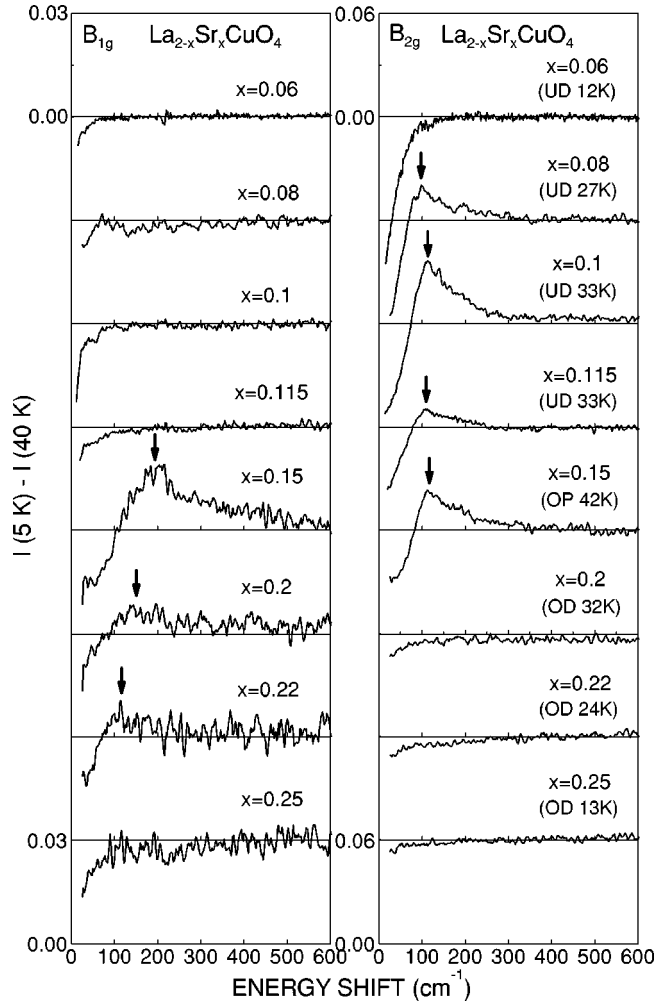
FIG. 4. Differential Raman spectra between 5 K and 40 K.

300 K to just above T_c is attributed to the formation of the pseudogap. The very small pseudogap in B_{2g} and the large pseudogap in B_{1g} is observed at $p=0.11$ in Bi2212 [Fig. 10(d)] consistent with ARPES. However, this situation is limited to this carrier density. The B_{2g} pseudogap opens at $p \geqslant 0.13$ in Bi2212 and in the whole carrier-density region in Bi2201. In LSCO the B_{1g} pseudogap does not open in the underdoped region. Thus the formation of the pseudogap depends on the material and the carrier density. The overall k-dependent density of states is already determined at 300 K and the change from 300 K to T_c is small. A large density of states enough to generate the superconducting gap structure is left in the B_{1g} pseudogap at T_c below $p < 0.15$ in LSCO and $p \leqslant 0.1$ in YBCO. Therefore the missing B_{1g} coherent peak at low carrier densities cannot be attributed to the formation of the pseudogap.

In the overdoped phase the density of states at $(\pi,0)$ becomes much larger than that at $(\pi/2,\pi/2)$. This is just like a formation of the large pseudogap at $(\pi/2,\pi/2)$. This carrier-density-dependent change of the electronic states cannot be explained by the hot spots and cold spots model. Recently it was found in overdoped Bi2212 that the scattering rate at $(\pi,0)$ does not increase in ARPES.[40] It is incon-

sistent with the hot spots model, but consistent with our results.

The common properties of the coherent peaks in these superconductors can be summarized as follows.

(1) The coherent peak appears typically in the B_{2g} spectra at low carrier densities and in the B_{1g} spectra at high carrier densities. The crossover occurs near the optimum doping, $p=0.16$, in LSCO and Bi2212, but it occurs at low carrier density, $p=0.1$ ($y=6.63$), in YBCO. In Bi2201 the B_{1g} coherent peak is always larger than the B_{2g} coherent peak. In Bi2212 and Bi2201 the B_{2g} coherent peak is large at the underdoped region, but both coherent peaks are observed in wide carrier density regions.

(2) The energy of the B_{1g} coherent peak is proportional to J^* in LSCO, Bi2212, and Bi2201. The proportionality coefficient is 0.37 in LSCO, 1.08 in Bi2212, and 0.94 in Bi2201 at the optimum doping. In YBCO the B_{1g} coherent peak energy decreases more rapidly than J^*, as carrier density increases, and becomes equal to J^* at the optimum doping. On the other hand, the B_{2g} coherent peak energy is much lower than J^* and not proportional to J^*.

(3) The low-energy scattering intensity increases gradually in B_{1g}, but decreases gradually in B_{2g}, as carrier density increases in the metallic region.

(4) The coherent peak height is reduced at $x=0.115$ in LSCO to form the (1/8)-stripe phase and around $y=6.63$ in YBCO to form the 60 K phase.

The superconducting gap energy determined from the B_{1g} coherent peak is strongly correlated with the effective exchange interaction energy. It suggests that the main origin of the superconductivity is the magnetic interaction. On the other hand, the B_{2g} coherent peak energy approaches the B_{1g} coherent peak energy from much lower energy, as the carrier density increases to the optimum doping. In the overdoped phase the B_{2g} coherent peak energy follows the B_{1g} coherent peak energy in Bi2212. It was pointed out that the B_{2g} coherent peak energy is related to T_c.[18,19] However, it is difficult to consider the reason that the gap energy around the node direction is determined by T_c, despite the monotonic decrease of the maximum gap energy at $(\pi,0)$ as carrier density increases. A more reasonable model can be considered in connection with the change of the electronic density of states in k space. That is, at low carrier densities the B_{2g} coherent peak represents the gap around $(\pi/2,\pi/2)$ with the large electronic density of states. As carrier density increases the component of the gap near $(\pi,0)$ increases instead of the decrease of the component around $(\pi/2,\pi/2)$. The carrier-density dependence of the B_{2g} coherent peak energy can be qualitatively explained by the change of the weight in the electronic density states from $(\pi/2,\pi/2)$ to $(\pi,0)$.

The coherent peak seems to appear in the symmetry in which the low-energy scattering intensity is larger, but the proportionality relation between their intensities is not observed. The exchange of the coherent peak height from B_{2g} to B_{1g} occurs in the narrow carrier-density region in spite of the gradual change of the low-energy scattering intensity in YBCO, LSCO, and Bi2212. It suggests that the coherent peak is not simply proportional to the density of states near
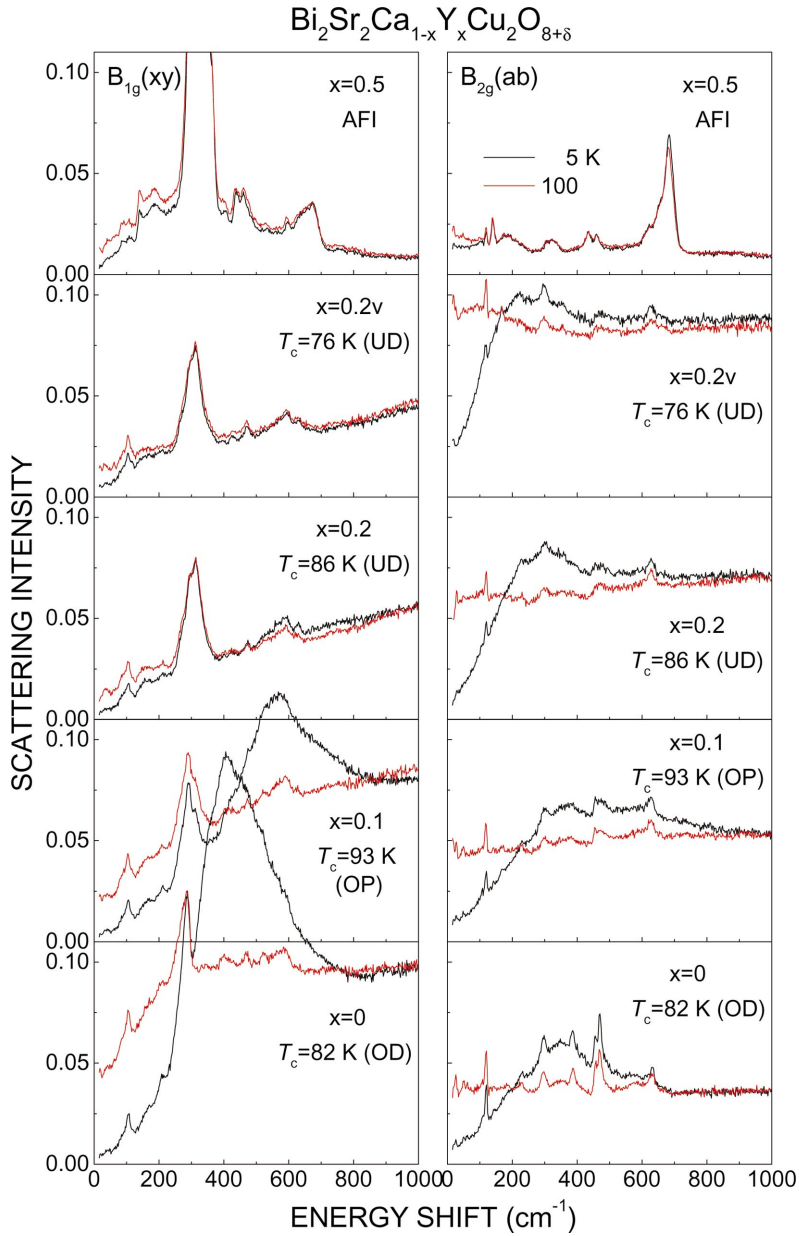
FIG. 5. (Color) B_{1g} and B_{2g} Raman spectra in Bi2212 at 5 K and 100 K.

E_F just above T_c. The coherent peak is generated only in the superconducting component of the electronic states as known from the fact that the coherent peak is not observed above T_c, even if the pseudogap opens, and it is sensitive to the (1/8)-problem in LSCO. Those experimental results suggest that some extra mechanism is necessary to sharpen the exchange of the coherent peak symmetry. Shen, Lanzara, Ishihara, and Nagaosa[41] calculated that the off-diagonal electron-phonon interaction of the zone-boundary LO mode at $(\pi,0)$ helps the spin-mediated superconductivity around $(\pi,0)$, but destroys the superconductivity around $(\pi/2,\pi/2)$. They did not discuss the effect of the LO mode at (π,π), but it is supposed that the (π,π) mode helps the spin-mediated superconductivity around $(\pi/2,\pi/2)$ and destroys the superconductivity around $(\pi,0)$. If the phonon mode with the strongest electron-phonon interaction changes from (π,π) to $(\pi,0)$ as carrier density increases, the rapid change of the coherent peak symmetry can be explained. In practice this change was observed in two-phonon Raman scattering as shown below.

IV. TWO-PHONON RAMAN SCATTERING

Usually two-phonon Raman scattering intensity is much smaller than single-phonon Raman intensity. However, in high-T_c superconductors the two-phonon scattering intensity is even larger than the single-phonon intensity in the AFI phase.[42–44] The large two-phonon scattering intensity is caused by the resonant Raman effect between the O(p)-Cu(d) charge transfer excitation and the incident light. Therefore the atomic vibrations in the CuO$_2$ planes are selectively enhanced. Figure 11 shows the A_{1g} phonon Raman spectra obtained from the (x,x), (a,a), (x,y), and (a,b) spectra by the calculation $[(x,x)+(a,a)-(x,y)-(a,b)]/2$. The peak energies at $x=0$ (0.15) are 128, 153(142), 194, (223), 226, 273(271), 307, 368(362), 396, 424(425), 460,

$Bi_2Sr_2Ca_{1-x}Y_xCu_2O_{8+\delta}$
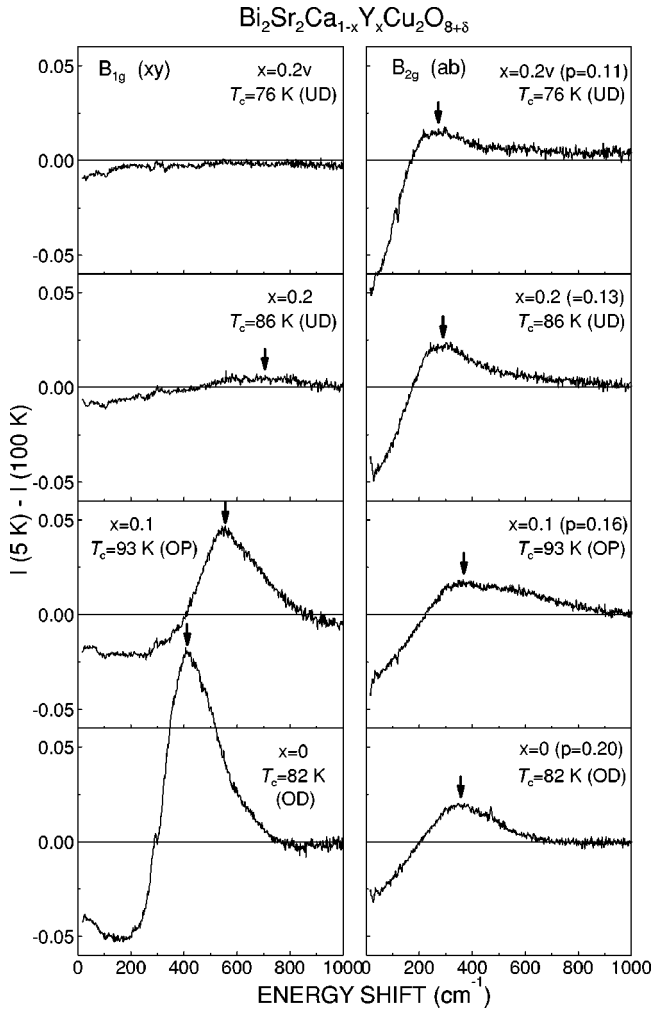
FIG. 6. Differential Raman spectra between 5 K and 100 K.

487(473), (529), 612, (612), 670(685), 708, 745(738), 873(833), 914, (935), 982, 1011, 1036, 1126(1065), 1171, 1226(1146), 1341(1267), 1426, 1446(1363) cm^{-1}. The peaks below 750 cm^{-1} come from mainly single-phonon scattering and those above it from two-phonon scattering. The A_{1g} mode energies in the tetragonal unit cell are 229 and 426 cm^{-1} at $x=0$.[42] The carrier-density dependence of the two-phonon peak energy is plotted in Fig. 12.

In the single-phonon process only $k\approx0$ modes are allowed from the momentum conservation among the phonon, incident light, and scattered light, while all modes in the Brillouin zone are allowed in the two-phonon process by the simultaneous creation of phonons at k and $-k$. Any symmetry mode becomes Raman active in the A_{1g} two-phonon scattering, because the irreducible representations reduced from the direct product of the same representations have the A_{1g} representation. The two-phonon scattering intensity is proportional to the fourth power of the electron-phonon interaction in the successive two-phonon creating process. There are two mechanisms for the strong two-phonon scattering in the AFI phase. The first is the Fröhlich-type electron-phonon interaction via macroscopic electric field accompanying $k\approx0$ LO phonons.[44] The second is especially strong electron-phonon interactions in the whole Brillouin zone.[43] These interactions include all interactions except for the Fröhlich-type interaction of $k\approx0$ LO phonons. Infrared active phonons are only $k\approx0$ modes from the momentum conservation between the phonon and light. Therefore infrared active $k\approx0$ A_{2u} and E_u modes can contribute only to the first mechanism.

It is expected that the Fröhlich interaction decreases rapidly as carriers are doped, because the electric field is screened by carriers. Recently Homes et al.[45] and Tu et al.[46] observed phonon spectra in the reflection spectra with the electric field perpendicular to the c axis at the optimally doped YBa$_2$Cu$_3$O$_{6.95}$ ($T_c=93$ K), Pr$_{1.85}$Ce$_{0.15}$CuO$_4$ ($T_c=19$ K), and Bi2212 ($T_c=91$ K). Tu et al.[46] argued that these modes are not the vibrations in the CuO$_2$ planes, but in the BiO and SrO layers. The oscillator strength in the infrared spectra is proportional to the square of the macroscopic electric field of the $k\approx0$ LO phonon. The appearance of the phonon structure indicates that the screening is poor for the electric field perpendicular to the c axis even in the metallic phase. However, the present Raman-scattering experiment shows that the two-phonon peaks of the infrared active modes decreases more rapidly than other two-phonon peaks as carrier density increases. It indicates that the Fröhlich-type electron-phonon interaction of the $k\approx0$ modes decreases more rapidly than the other electron-phonon interactions of large k modes. The Fröhlich-type electron-phonon interaction for the $k\approx0$ infrared active modes does not contribute to the superconductivity.

The upper panel of Fig. 13 shows the high-energy part (1050–1500 cm^{-1}) of the two-phonon Raman spectra in the AFI phase ($x=0$ and 0.035) and the boundary of the metallic phase ($x=0.06$). The middle panel is the spectra in the range of half the energy (525–750 cm^{-1}). The spectra in this range are composed of single-phonon scattering and two-phonon scattering. The lower panel is the optical conductivity $\sigma(\omega)$ and the loss function $-\mathrm{Im}[1/\epsilon(\omega)]$ obtained from the Kramers-Kronig transformation of the infrared-ultraviolet reflection spectra of the same La$_2$CuO$_4$ crystal. The electric field of light is perpendicular to the c axis. The wide-energy-range reflection spectra were obtained by connecting the measured reflection spectra from 50 cm^{-1} to 6 eV and the reported vacuum-ultraviolet spectra from 6 eV to 35 eV.[47] The higher-energy expansion is followed by the formula of $R(\omega)\propto\omega^{-4}$. The E_u transverse-optical (TO) phonon energies obtained from the peaks in $\sigma(\omega)$ are 151, 184, 361, and 680 cm^{-1} at 20 K, if we ignore the splitting by the orthorhombic distortion. The corresponding LO phonon energies obtained from the $-\mathrm{Im}[1/\epsilon(\omega)]$ are 168, 275, 460, and 712 cm^{-1}. Many energies are consistent with the reported results.[48,49] The reported energies of the TO(LO) A_{2u} phonons are 150(150), 230(458), and 512(575) cm^{-1}.[50–52] These modes have polarizations parallel to the c axis. As shown in the upper panel of Fig. 13, the 1426 cm^{-1} peak has a shoulder at 1446 cm^{-1}. The 1426 cm^{-1} energy is twice the E_u (LO) phonon energy 712 cm^{-1}. The intensity of the peak decreases rapidly as carrier density increases to $x=0.035$. This peak is assigned to the two-phonon peak of the 712 cm^{-1} E_u (LO) phonon mode. The corresponding single-
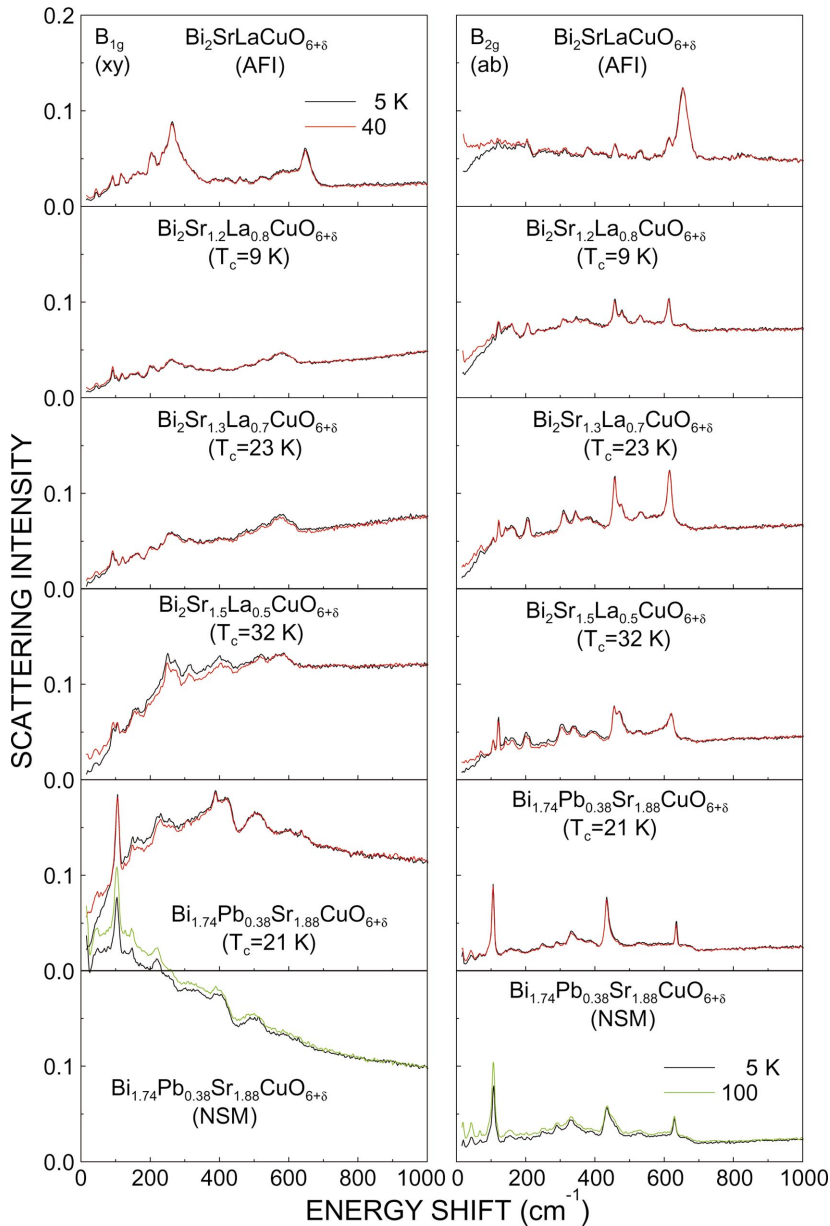
FIG. 7. (Color) B_{1g} and B_{2g} Raman spectra in Bi2201 at 5 K and 40 K (100 K in nonsuperconducting metallic $Bi_{1.74}Pb_{0.38}Sr_{1.88}CuO_{6+\delta}$).

phonon Raman peak is observed at 708 cm^{-1}. The intensity of this peak also decreases as carrier density increases and almost disappears at $x=0.08$. The crystal structure of LCO is D_{2h}^{18}. This structure has inversion symmetry and the Raman activity and the infrared activity are exclusive. The possible mechanism for the Raman scattering of the infrared active mode is the intraband Fröhlich interaction at the resonant Raman condition.[53,54] The possibility of the imperfection-induced mechanism is removed because the intensity decreases as Sr concentration increases.

The energy of the 1171-cm^{-1} peak is twice the energy of the A_{2u} (LO) phonon (575 cm^{-1} at room temperature).[50] The intensity of this peak decreases rapidly as carrier density increases. The 1171-cm^{-1} peak is assigned to the two-phonon peak of the A_{2u} (LO) phonon mode. The single-phonon peak is not observed, because the Raman spectra were measured in the (a,a), (a,b), (x,x), and (x,y) polarization configurations which do not include the c axis. The

914-cm^{-1} peak is assigned to the two-phonon peak of the 460-cm^{-1} E_u (LO) phonon mode. The 460-cm^{-1} peak in Fig. 11 is the single-phonon Raman peak. They also decrease rapidly as carrier density increases.

The most dominant peak in the underdoped phase is the 1446-cm^{-1} ($x=0$) peak. It decreases gradually as carrier density increases and the 1146-cm^{-1} ($x=0.15$) peak becomes the most dominant peak in the optimally-doped and overdoped phases. The energy at $x=0$ is 1226 cm^{-1}. This mode is likely not to be the $k\approx0$ mode, because the corresponding single-phonon peak is not observed at $k\approx0$.

Pintschovius and co-workers[48,55,56] found by neutron scattering that there are two distinct phonon modes whose energies decrease sensitively as carrier density increases. Those modes are the highest-energy Δ_1 mode around $(\pi,0)$ (half-breathing mode) and the Σ_1 mode around (π,π) (breathing mode) on the E_u (LO) mode (at $k=0$) branch. The energies decrease from 636 cm^{-1} at $x=0$ to 553 cm^{-1} at $x=0.15$ for
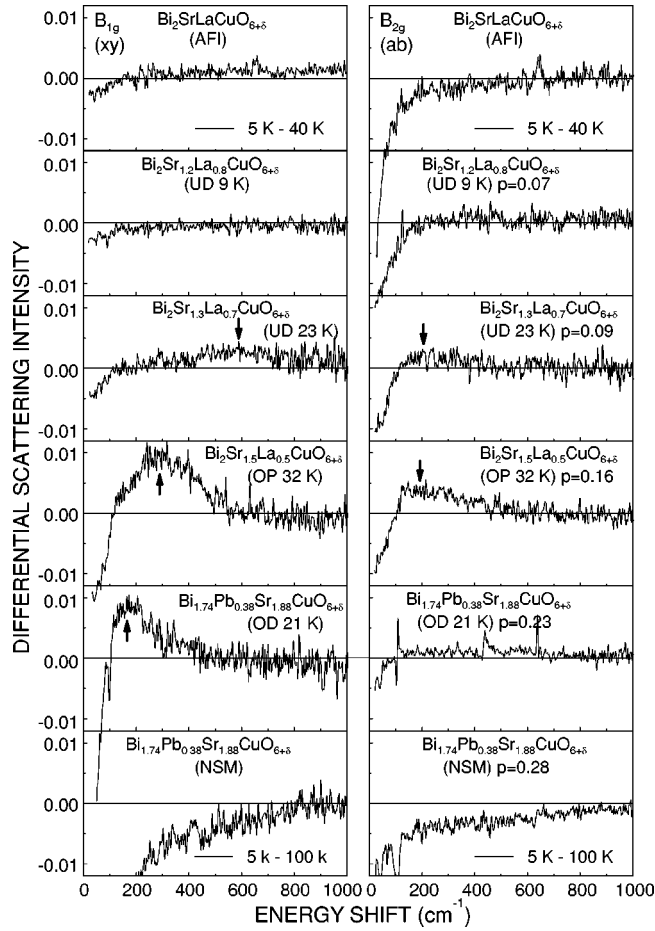
FIG. 8. Differential Raman spectra between 5 K and 40 K (100 K in $Bi_{1.74}Pb_{0.38}Sr_{1.88}CuO_{6+\delta}$).

the Δ_1 $(\pi,0)$ mode and 722 cm^{-1} at $x=0$ to 667 cm^{-1} at $x=0.15$ for the Σ_1 (π,π) mode. Twice the energies are plotted in Fig. 12. From the coincidence of the energy, the 1200-cm^{-1} and 1400-cm^{-1} two-phonon branches in Fig. 12 are assigned to the Δ_1 mode at $(\pi,0)$ and Σ_1 mode at (π,π), respectively. Falter and co-workers[57–61] showed that the carrier-induced softening is reproduced by long-range, nonlocal electron-phonon interaction effects of charge fluctuation within the framework of a local-density approximation. They also calculated that the 425-cm^{-1} Δ_1 mode at $(\pi,0)$ in the metallic phase has large electron-phonon interactions.[57,58] The 900-cm^{-1} branch in Figs. 11 and 12 can be assigned to the two-phonon scattering of this mode. The corresponding mode in YBCO was attributed to the interaction with the A_g phonon branch by Pintschovius and Reichardt[55] and to the stripe effects by Mook and Doğan.[62] The anomalous dispersion of the LO phonon on the $(q,0)$ direction in $La_{0.85}Sr_{0.15}CuO_4$ (Ref. 63) is controversial.[56]

The intensity of the two-phonon peak of the Σ_1 (π,π) mode decreases monotonically from $x=0$ to $x=0.15$, as carrier density increases. On the other hand, the intensity of the two-phonon peak of the Δ_1 $(\pi,0)$ mode increases at $x \geqslant 0.1$. The relative intensity of the 1200-cm^{-1} peak to the sum of the 1200- and 1400-cm^{-1} peaks is shown in Fig. 14. The crossover carrier density, $x=0.115–0.15$, is in good ac-

cordance with the carrier density $x=0.15$ for the $(\pi/2,\pi/2)$ $-(\pi,0)$ crossover of the coherent peak as presented in the preceding section. The momentum crossover of the strongest electron-phonon-interaction mode is commonly observed in high-T_c superconductors, although the crossover carrier density and the overlap region depend on the compounds. McQueeney and coworkers[64] observed the appearance of the 70-meV (580-cm^{-1}) mode in the metallic phase above x =0.06 by neutron scattering. The present Raman-scattering experiment disclosed that the mode continues from $x=0$. The energy decreases from 613 cm^{-1} at $x=0$ to 604 cm^{-1} at $x=0.06$, 575 cm^{-1} at $x=1.0$ and 573 cm^{-1} at $x=0.15$.

The Σ_1 (π,π) and the Δ_1 $(\pi,0)$ two-phonon peaks have different temperature dependence in the underdoped region. Figure 15 shows the temperature dependence of the two-phonon spectra at four carrier densities. At $x=0$, 0.15, and 0.2 the decreasing rates of the Σ_1 two-phonon peak and the Δ_1 two-phonon peak are nearly the same, while at $x=0.1$ the Δ_1 two-phonon peak decreases more rapidly than the Σ_1 two-phonon peak as temperature increases from 5 K to 300 K. The same temperature dependence is observed commonly in the underdoped region at $x=0.06$ and 0.115.

Figure 16 shows the phonon Raman spectra in YBCO at 60 K. The peak energies in $y=6.33(6.91)$ are 87(89), 117(116), 144(151), 191(193), 268(265), 453(443), 485(504), 554, 582(584), 796, 1296 cm^{-1}. The energies of large peaks are consistent with reported energies, for example, 115, 145, 454, and 472 at $y=6$.[65] The large peak changes from the 142-cm^{-1} $(y=6.2)$ peak to the 116-cm^{-1} $(y=6.91)$ peak at $y=6.63–6.83$. The 116-cm^{-1} $(y=6.91)$ peak splits into two peaks at $y=6.46–6.83$. Another large peak changes from the 454-cm^{-1} $(y=6.2)$ peak to the 504-cm^{-1} $(y=6.91)$ peak at $y=6.33–6.46$. The strongest two-phonon peak is observed at 1296 cm^{-1} in the AFI phase $(y=6.2)$. This peak decreases in energy and intensity as carrier density increases from y =6.2 to $y=6.63$. The origin of the sharp peaks near 1220 cm^{-1} marked by asterisks at $y=6.54$, 6.63, and 6.83 is not the intrinsic mode, but the mode in the reconstructed layer on the cleaved surface. The large cusp at 300 cm^{-1} in $YBa_2Cu_3O_{6.91}$ is the superconducting gap structure.

Figure 17 shows the selected spectra in the photobleaching process of reconstructed layer modes at $y=6.83$. The surface was cleaved in air at room temperature and set in the cryostat followed by cooling to 5 K in helium gas without illumination. The Raman spectra were measured on the same spot successively at 5, 20, 40, 60, 80, 100, 150, 200, 250, and 300 K on heating. The duration is 2 h for each scan. The laser power was 20 mw/(50×500) μm^2. The spectra did not change by the illumination of laser light at 5 K, but at 20–100 K the peaks at 235, 266, 292, 309, 593, 634, 781, 883, 1058, 1178, 1194, 1264, 1422, 1493, 1654, 1772, 1857, and 2017 cm^{-1} (5 K) decreases by illumination. These peaks are due to the modes in the reconstructed layer. Above 150 K these peaks increase again. Figure 16 was obtained after the illumination of laser light at 20 K so as to reduce the intensity of the 1220-cm^{-1} peak below about 1/20. The other two-phonon peaks in the two-phonon scattering region of Fig. 16 seem to be intrinsic, because the spectra are nearly
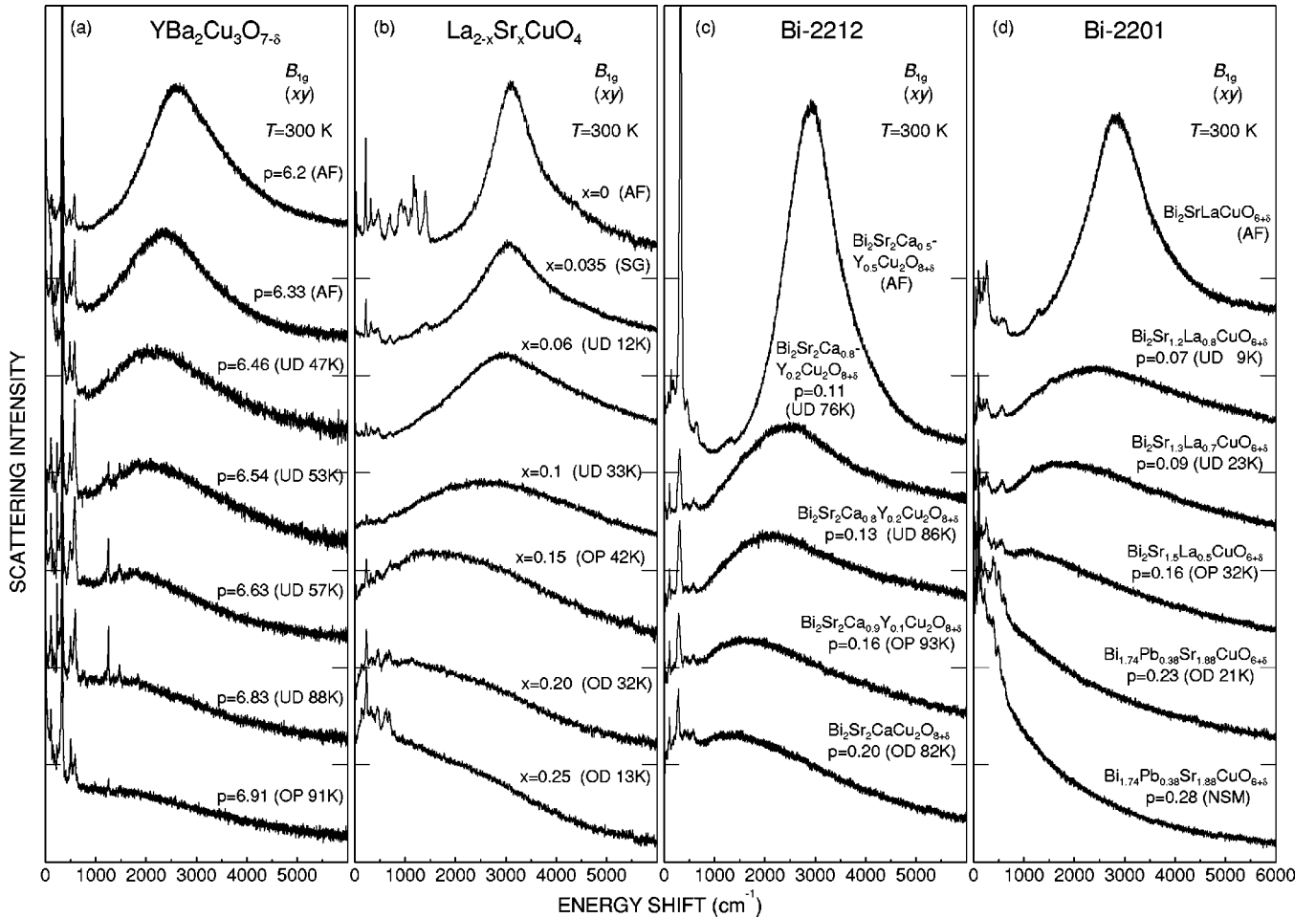
FIG. 9. B_{1g} spectra in YBCO, LSCO, Bi2212, and Bi2201 at 300 K.

the same as the 100-K spectra in which the 1220-cm^{-1} peak almost disappears.

In order to assign the origin of the two-phonon peaks, the Raman spectra are plotted in the single-phonon scale as well as the two-phonon scale in Fig. 18. There is no single-phonon peak corresponding to the 1296-cm^{-1} two-phonon peak. Many experiments of infrared spectroscopy were made.[49,66–69] The TO (LO) phonon energies of the infrared active A_{2u} modes are 105(110), 146(180), 215(222), 367(470), and 645(664) and those of the E_u modes are 116(125), 188(199), 246(266), 351(420), and 595(637) at $y = 6$.[66] Infrared active modes are usually screened by the itinerant carriers in metal. However, it was reported that the electric fields of the E_u modes are not screened and can be observed in the metallic phase.[45] The TO phonon energies 250, 357, and 588 cm^{-1} at $y = 6.1$ (Ref. 49) change to 275, 360, and 581 cm^{-1} at $y = 6.95$.[45] The small carrier-density dependence of the highest-energy E_u mode is consistent with the neutron-scattering experiment that the LO phonon energy at $k \approx 0$ changes from 594 cm^{-1} at $y = 6$ to 580 cm^{-1} at $y = 7$.[48] On the other hand, the neutron-scattering experiment showsed that the energy of the Σ_1 (π,π) mode decreases from 687 cm^{-1} at $y = 6$ to 610 cm^{-1} at $y = 7$.[48] The energy of the two-phonon Raman peak changes from 1296 cm^{-1} at $y = 6.2$ to 1241 cm^{-1} at $y = 6.46$. Therefore the 1295-cm^{-1}

two-phonon peak does not come from the E_u (LO) mode, but from the Σ_1 (π,π) mode. This two-phonon peak can be observed till $y = 6.63$. The Raman spectra have no dominant two-phonon peak at $y > 6.63$. Recent neutron-scattering experiments showed that the Δ_1 phonon dispersion is very anisotropic along the a axis and the b (chain) axis in the orthorhombic phase.[70,71] The Δ_1 mode energies at $y = 6.6$ are 393, 461, and 582 cm^{-1} at ($\pi,0$) and 411, 461, and 463 cm^{-1} at ($0,\pi$). The Δ_1 mode energies at $y = 7$ are 145, 223, 265, 391, 465, and 523 cm^{-1} at ($\pi,0$) and 147, 221, 265, 417, 447, and 452 cm^{-1} at ($0,\pi$). The large anisotropy may cause difficulty in producing a large two-phonon peak. The large dispersion of the Δ_1 mode causes complex mode crossing. The energies of the ($\pi,0$) and ($0,\pi$) modes are shown in Fig. 18. The correlation between these energies and the two-phonon peak energies is not observed.

The disappearance of the Σ_1 (π,π) two-phonon peak occurs at the 60-K phase. It is very different form the case of LSCO in which the crossover of the dominant two-phonon peak from Σ_1 (π,π) to Δ_1 ($\pi,0$) occurs at the optimum carrier density $x = 0.15$. This difference seems to be related to the difference of the carrier density for the momentum crossover of the superconducting coherent peak from ($\pi/2,\pi/2$) to ($\pi,0$).

Figure 19 shows the A_{1g} phonon Raman spectra in
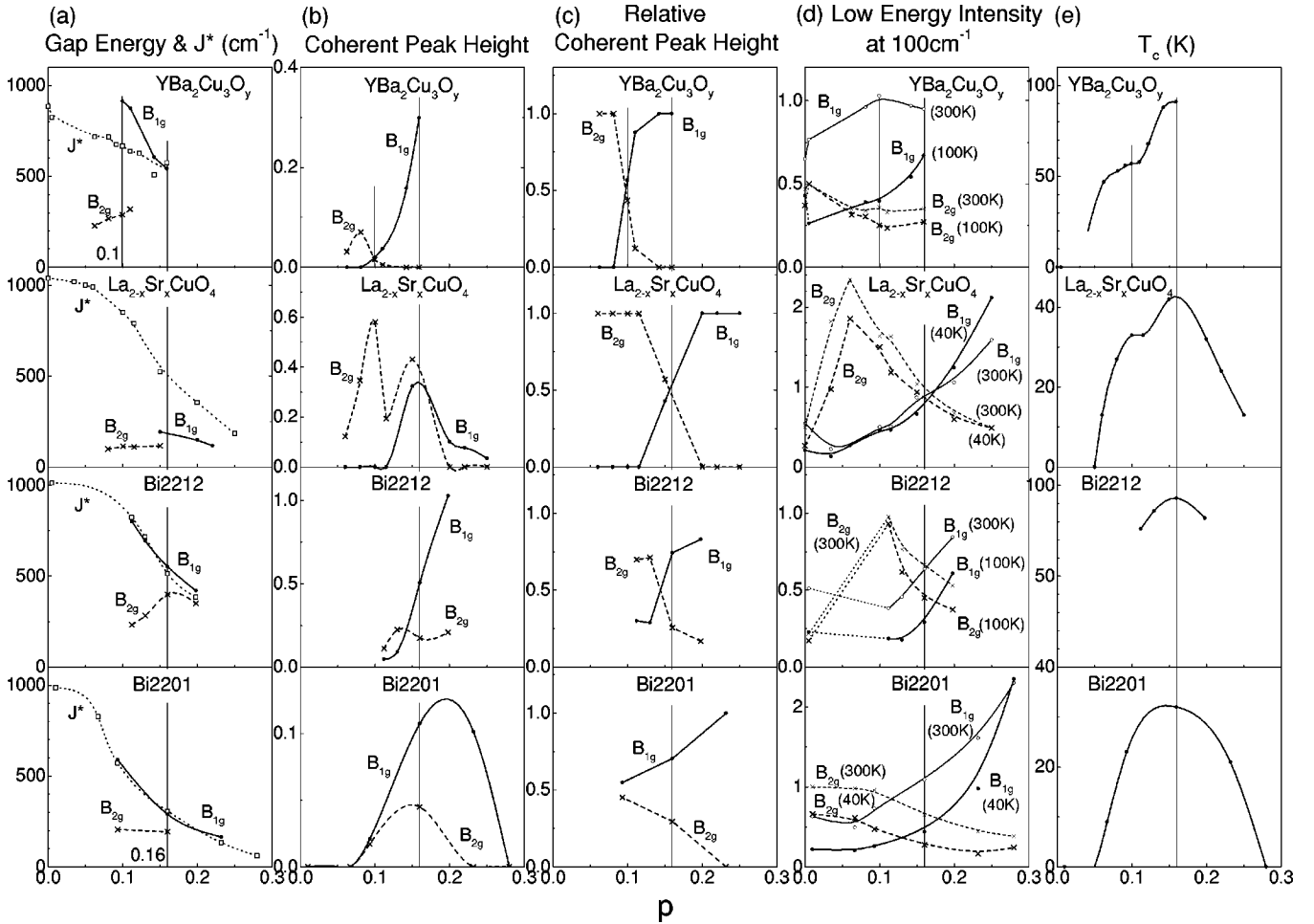
FIG. 10. (a) B_{1g} and B_{2g} coherent peak energies and the effective exchange interaction energies J^* obtained from two-magnon peak energies; (b) B_{1g} and B_{2g} coherent peak heights; (c) relative coherent peak height between B_{1g} and B_{2g}; (d) low-energy electronic Raman intensity at 100 cm^{-1} at 300 K and just above T_c; and (e) T_c. The B_{1g} electronic Raman spectra represent the excitations around $(\pi,0)$ and the B_{2g} spectra represent the excitations around $(\pi/2,\pi/2)$. The increase of the B_{1g} low-energy scattering intensity in YBCO from 100 K to 300 K is caused by the increase of the extrinsic phonon scattering in the reconstructed surface layer on the cleaved surface.

Bi2212 at 5 K. The peak energies in AFI Bi$_2$Sr$_2$Ca$_{0.5}$Y$_{0.5}$Cu$_2$O$_{8+\delta}$ [overdoped superconducting Bi$_2$Sr$_2$CaCu$_2$O$_{8+\delta}$ (OD 82K)] are 62(61), 86(109), 120(120), 139(128), (172) 188(185), 202(198), 231, 311(297), 331(324), 378(360), (388), 436(412), 460(457), 474(470), (524), (556), 624(632), 683(663), 870, 1130, 1312, and 1378 cm^{-1}. The energies of many modes are consistent with the reported energies.[72–74] The orthorhombic distortion and the incommensurate structural modulation reduce the crystal symmetry and increase phonon modes at $k \approx 0$. The strong peaks at 139, 436, 460, and 683 cm^{-1} in the AFI phase rapidly decrease in intensity, when the material becomes metallic in Bi2212 (UD 76 K). The change induced by the Y substitution is also observed in the phonon density of states measured by neutron scattering.[75] The cusp structure at 300 cm^{-1} in Bi$_2$Sr$_2$CaCu$_2$O$_{8+\delta}$ (OD 82 K) is the A_{1g} superconducting gap structure. Many infrared reflection experiments have been reported.[46,76,77] The TO(LO) phonon energies in Bi$_2$Sr$_2$CaCu$_2$O$_{8+\delta}$ (OP 91 K) for the electric field parallel to the c axis ($E \| c$) are 93(96), 164(172), 208(213), 281(284), 304(328), 360(379), 460(464), 521(527), 584(629), and 625(652) cm^{-1} at 295 K.[46] The TO phonon

energies for $E \| a$ are 473 and 613 cm^{-1}. The TO phonon energies for $E \| b$ are 325 and 613 cm^{-1}. The LO phonon energies were not explicitly reported. These modes measured with $E \| a$ and $E \| b$ were assigned to the vibrations in the BiO and SrO layers.[46] The A_{1g} phonon energies in Bi$_2$Sr$_2$CaCu$_2$O$_{8+\delta}$ (OD 82 K) at 300 K in the present experiment are 60, 107, 118, 127, 184, 295, 323, 355, 388, 408, 468, 627, and 660 cm^{-1}. There is no clear coincidence between Raman active phonons and infrared active phonons.

In order to search single-phonon peaks corresponding to the two-phonon peaks, the Raman spectra were plotted simultaneously in the single-phonon scale and the two-phonon scale in Fig. 20. The 1378-cm^{-1} two-phonon peak in AFI phase has the corresponding single-phonon peak at 683 cm^{-1}. Both peaks rapidly decrease in intensity as the material becomes metallic. The single-phonon energy decreases from 683 cm^{-1} in AFI to 664 cm^{-1} in Bi2212 (UD 76 K). This phonon is possibly the in-plane E_u (LO) phonon mode at $k \approx 0$. The 1312-cm^{-1} two-phonon peak has no corresponding single-phonon peak. Therefore this peak is assigned to the mode with a large wave vector. The possible
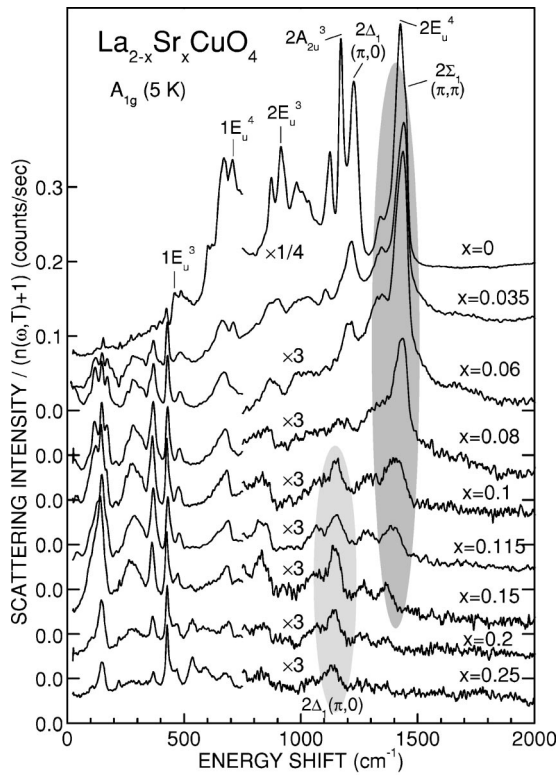
FIG. 11. A_{1g} two-phonon Raman spectra in LSCO. The dark gray area indicates that the two-phonon peak of the (π,π) LO mode is strong and the light gray area indicates that the two-phonon peak of the $(\pi,0)$ LO mode is strong.
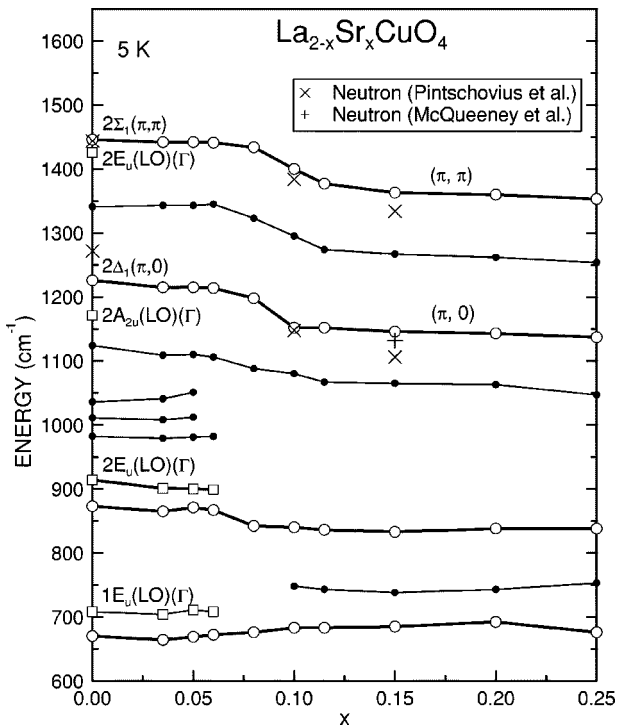
FIG. 12. The carrier-density dependence of two-phonon peak energies above 750 cm^{-1} and the one-phonon peak energies below 750 cm^{-1}. The dominant branches in the optimally doped region are shown by thick lines and open circles. The crosses are neutron data (Refs. 48, 55, 56, 63).
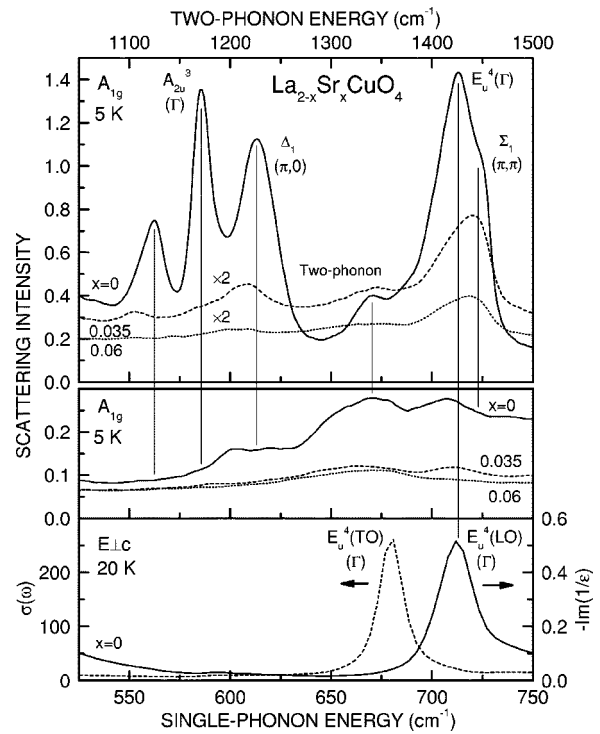
FIG. 13. Upper panel: the A_{1g} two-phonon Raman spectra at $x = 0$, 0.35, and 0.6. Middle panel: the A_{1g} Raman spectra in the half-energy range of the upper panel. Lower panel: the optical conductivity and the loss function of La$_2$CuO$_4$.

mode is the Σ_1 mode at (π,π) from the analogy of LSCO. The two-phonon peak decreases in intensity as carrier density increases. The peak can be observed till Bi2212 (OP 93 K) in Fig. 19. A broad kink appears around 1050 cm^{-1} in Bi2212 (OD 82 K). In the case of Bi2201 [OD 21 K and no superconducting metal (NSM)] a cusp appears near this energy. The carrier density 0.2/Cu in Bi2212 (OD 82 K) is smaller than the carrier density 0.23 in Bi2201 (OD 21 K) and 0.28 Bi2201 (NSM). It is expected that the broad kink in Bi2212 changes to a cusp, if carrier density increases. It is
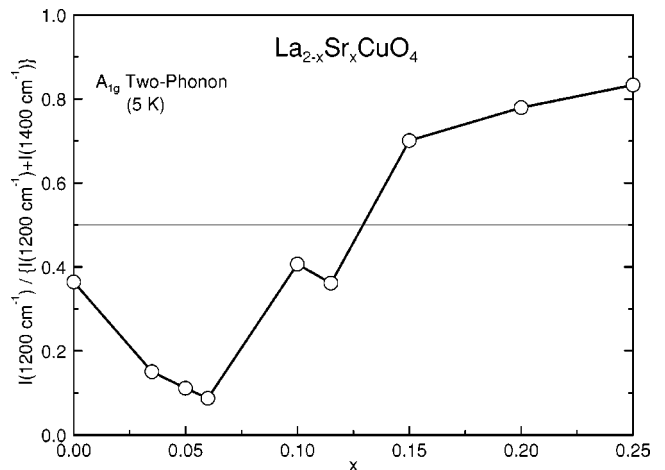
FIG. 14. Relative integrated intensity of the $(\pi,0)$ two-phonon peak near 1200 cm^{-1} to the sum of the $(\pi,0)$ two-phonon peak and the (π,π) two-phonon peak near 1400 cm^{-1}.
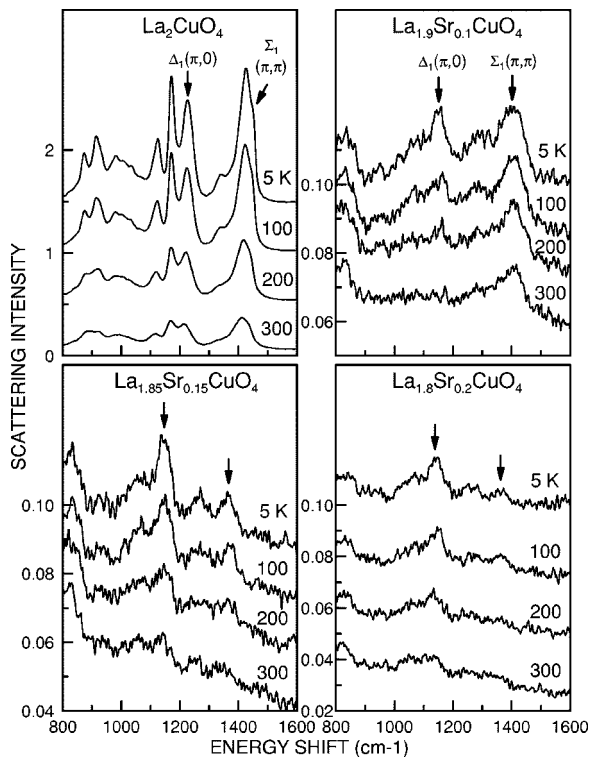
FIG. 15. Temperature dependence of the two-phonon Raman spectra at $x=0$, 0.1, 0.15, and 0.2 in LSCO.

FIG. 16. A_{1g} two-phonon Raman spectra in YBCO.
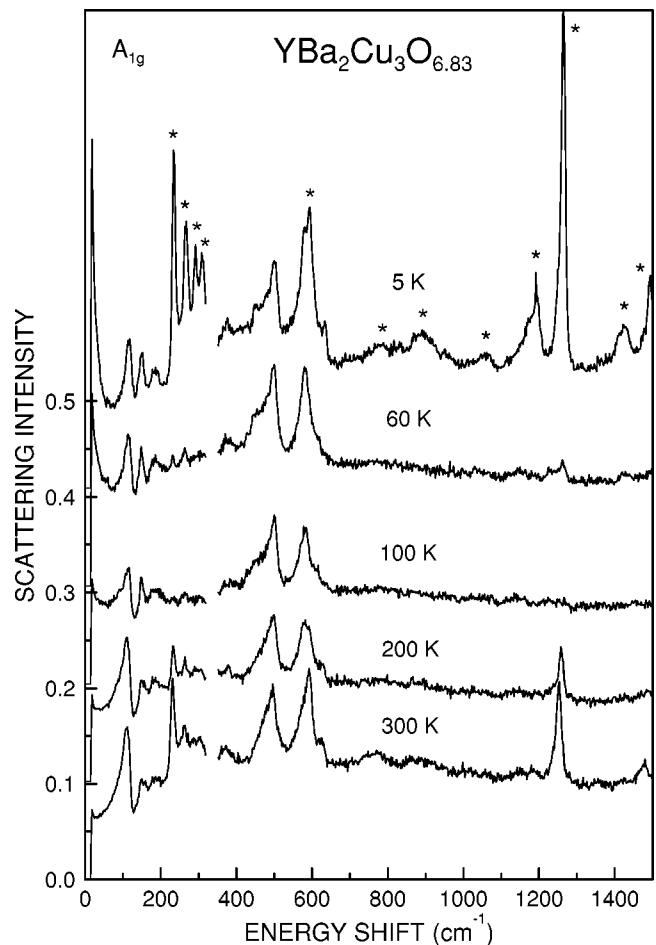
FIG. 17. Photobleaching process of Raman peaks in the reconstructed surface layer. Raman spectra were measured successively at 5, 20, 40, 60, 80, 100, 150, 200, 250, 300 K on heating. The duration for each spectra was 2 h.
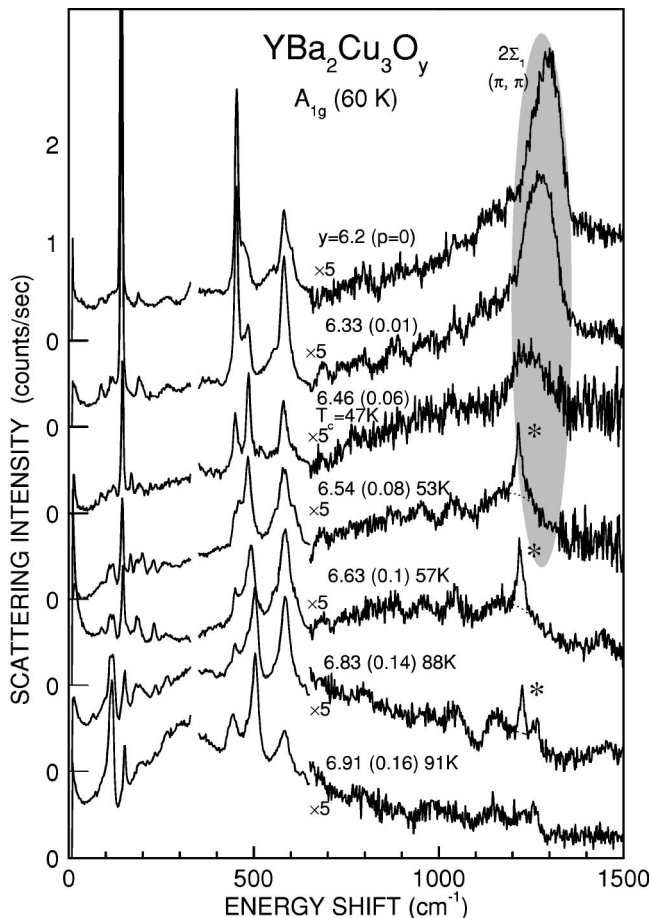
supposed that the kink and cusp are due to the two-phonon scattering of the Δ_1 phonon at $(\pi,0)$ from the analogy of LSCO.

Figure 21 shows the A_{1g} Raman spectra of Bi2201 at 5 K. The peak energies in AFI $Bi_2SrLaCuO_{6+\delta}$ (optimally doped superconducting $Bi_2Sr_{1.5}La_{0.5}CuO_{6+\delta}$, OP 32 K) are 71(70), 99(107), 123(122), 175(162), 206(202), 244(251), 314(311), 327, 351(336), 379(391), 408(406), 459(457), 478(471), (519), 531, 549, (585), 615(622), 652(667), (752), 828, 905, (985), 1067, (1100), 1202, 1317 cm^{-1}. Some peaks change by the Pb substitution. The peak energies in $Bi_{1.74}Pb_{0.38}Sr_{1.88}CuO_{6+\delta}$ (OD 21 K) are 44, 68, 78, 107, 116, 160, 181, 203, 217, 260, 292, 331, 360, 391, 464, 532, 592, 635, 664, 1094 cm^{-1}. The energies of many modes are consistent with the reported energies.[73,78] The TO(LO) phonon energies in ($Bi_2Sr_2CuO_{6+\delta}$, $T_c=6-8$ K) for the electric field parallel to the c axis are 87(116), 149(175), 198(218), 307(330), 391(427), 462(463), 596(626), and 644(655) cm^{-1} at 8 K.[77]

Figure 22 shows the Raman spectra in the single-phonon scale and the two-phonon scale. The energy of the 652-cm^{-1} peak is near half the energy of the 1317-cm^{-1} two-phonon peak. The intensity of the 652-cm^{-1} peak rapidly decreases
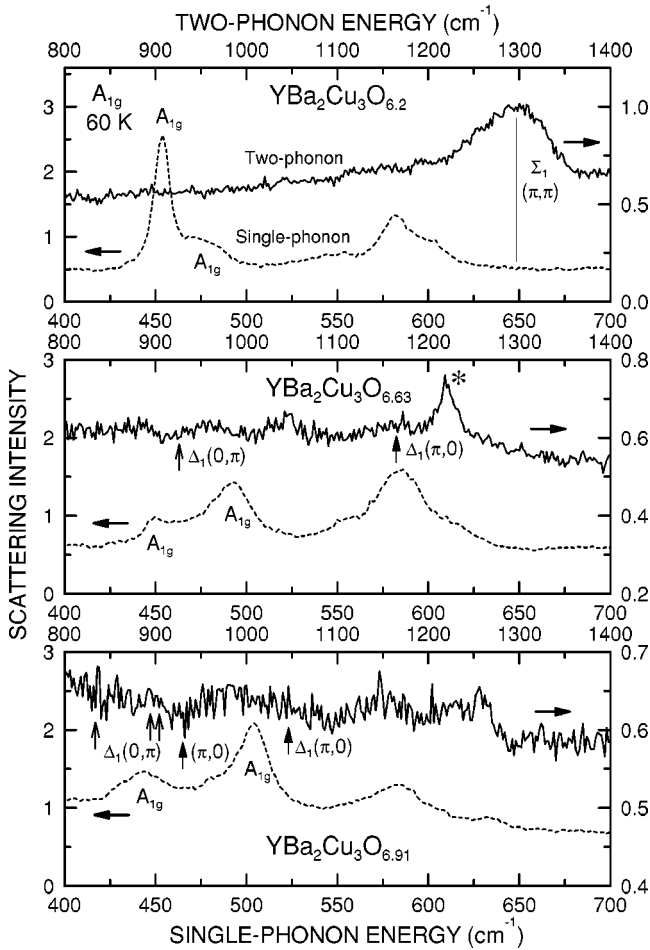
FIG. 18. A_{1g} Raman spectra plotted in the single-phonon scale (solid line) and the two-phonon scale (dashed line).

FIG. 19. A_{1g} two-phonon Raman spectra in Bi2212.

like the 683-cm^{-1} peak in Bi2212 (AFI) as the material changes into metal. This phonon energy is close the 655 cm^{-1} energy of the A_{2u} LO phonon at $k \approx 0$. However the A_{2u} phonon is not easily screened even in the metallic phase. The rapid decrease suggests that this mode is possibly the in-plane E_u (LO) phonon at $k \approx 0$. The energy of the single-phonon peak increases from 652 cm^{-1} in Bi2201 (AFI) to 663 cm^{-1} in Bi2201 (UD 9 K), but the energy of the two-phonon peak decreases from 1317 cm^{-1} to 1302 cm^{-1}. Therefore the two-phonon peak in Bi2201 (UD 8 K) does not contain the 663-cm^{-1} E_u phonon component. It is supposed from the analogy of LSCO that the two-phonon peak is produced by the Σ_1 mode at (π,π). The 1317-cm^{-1} peak in AFI is composed of the Σ_1 (π,π) mode and the 652-cm^{-1} E_u ($k \approx 0$) mode. The broad two-phonon peak at 1097 cm^{-1} in Bi2201 (NSM) has no corresponding single-phonon peak. It is supposed that the origin of this peak is the Δ_1 mode at $(\pi,0)$. As shown in Fig. 21 the 1317-cm^{-1} (AFI) two-phonon peak decreases in intensity from AFI to Bi2201 (UD 23 K). The most dominant two-phonon peak in Bi2201 (UD 23 K) and Bi2201 (OP 32 K) is the 981-cm^{-1} (OP 32 K) peak. The 1097 cm^{-1} (NMS) two-phonon peak emerges in Bi2201 (UD 23 K) and becomes the only one two-phonon peak in Bi2201 (OD 21 K) and (NSM).

In Bi2212 the dominant two-phonon peak changes from
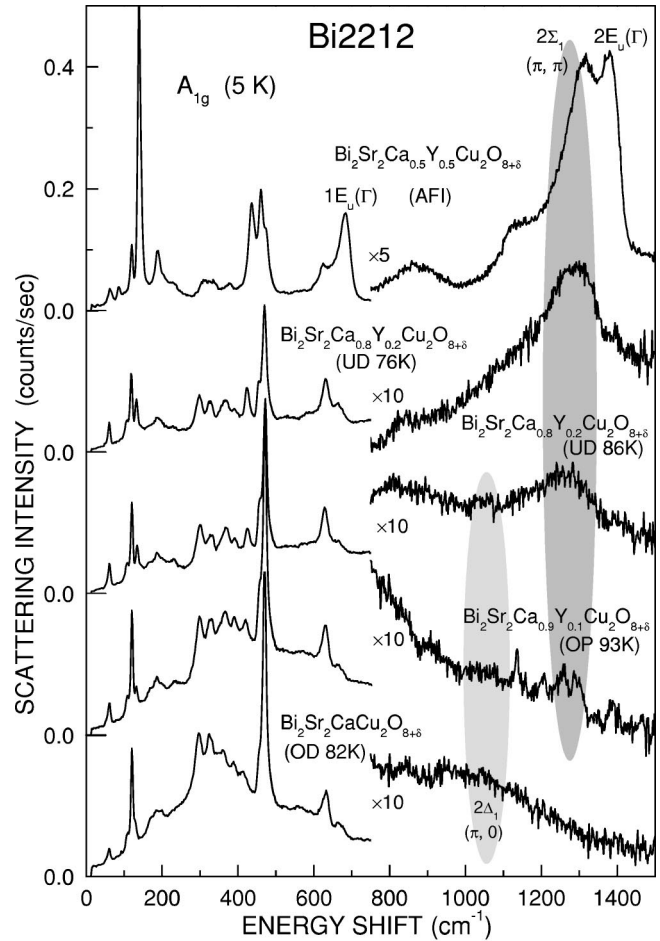
(π,π) to $(\pi,0)$ at $p=0.16$. On the other hand, in Bi2201 the crossover occurs at $p=0.09$. The overlap range is large. The relative intensity of the two-phonon peak of the Δ_1 $(\pi,0)$ mode to that of the Σ_1 (π,π) mode is larger in Bi2201 than in Bi2212 at the same carrier density. These differences are reflected to the crossover behavior of the superconducting coherent peak. The B_{2g} coherent peak at $(\pi/2,\pi/2)$ is not observed in overdoped Bi2201, while it is observed from the underdoped region to the overdoped region in Bi2212. The B_{1g} coherent peak at $(\pi,0)$ is stronger than the B_{2g} coherent peak even in the underdoped region in Bi2201.

The typical carrier-density dependence of the electronic states is shown in Fig. 23. The thick parts of the Fermi surface indicate the position with the large electronic density of states above T_c. The area of the large electronic density of states shifts gradually from $(\pi/2,\pi/2)$ to $(\pi,0)$ as carrier density increases. The position of the superconducting coherent peak moves from $(\pi/2,\pi/2)$ to $(\pi,0)$ in the same way as the change of the electronic density of states, but the change occurs in rather narrow carrier-density width. According to the change of the coherent peak position the momentum of the phonon mode with the strongest electron-phonon interactions changes from (π,π) to $(\pi,0)$. It strongly suggests that the Σ_1 (π,π) LO phonon helps pair creation at $(\pi/2,\pi/2)$ and causes pair breaking at $(\pi,0)$ in the underdoped region
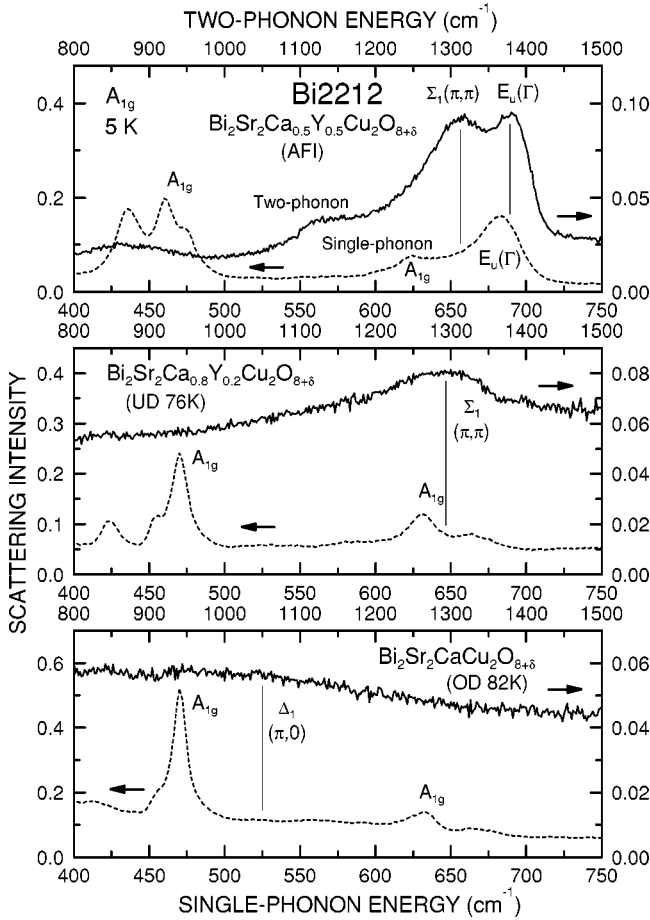
FIG. 20. A_{1g} Raman spectra plotted in the single-phonon scale (solid line) and the two-phonon scale (dashed line).

FIG. 21. A_{1g} two-phonon Raman spectra in Bi2201.

and the Δ_1 $(\pi,0)$ LO phonon helps pair creation at $(\pi,0)$ and causes pair breaking at $(\pi/2,\pi/2)$ in the overdoped region. This zone-boundary LO phonon-induced anisotropic enhancement and reduction of the superconductivity is consistent with the calculation by Shen, Lanzara, Ishihara, and Nagaosa.[41] It should be noticed that the superconducting gap energy determined from the B_{1g} coherent peak energy follows the effective exchange interaction energy. It indicated that the main mechanism for the high-T_c superconductivity is the magnetic interaction. If the phonon modes directly mediate the pairing, the phonon peak should be very broad as in MgB_2.[79-81]

The energies of the phonon modes at $(\pi,0)$ are 570 cm^{-1} in LSCO, 525 cm^{-1} in Bi2212, and 550 cm^{-1} in Bi2201. These energies are close to the energies, 70 meV (560 cm^{-1}), at which kinks are observed in the electronic dispersion curves in ARPES.[24,41,82-86] The dispersion changes below T_c near the kink and the coherent peak appears unexpectedly even along the node direction (0, 0)-(π,π). Two main possible excitations coupled with the electronic states have been pointed out for the origin of the kink. One is the phonon at $(\pi,0)$ (Refs. 41,82) and the other is the collective magnetic excitation at (π,π).[85] The present Raman scattering favors the phononic origin, because this phonon is found to couple strongly with electronic states and play the important role for the superconductivity.
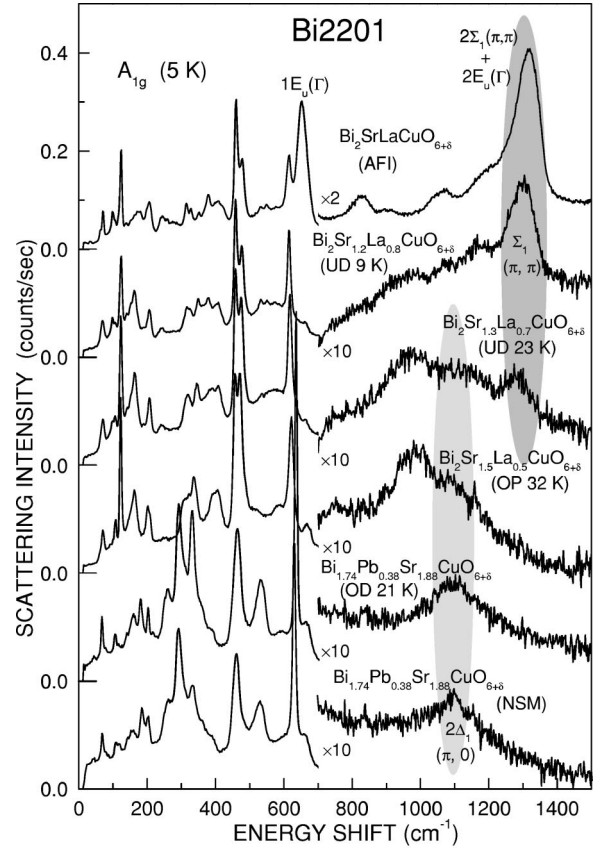
FIG. 22. A_{1g} Raman spectra plotted in the single-phonon scale (solid line) and the two-phonon scale (dashed line).
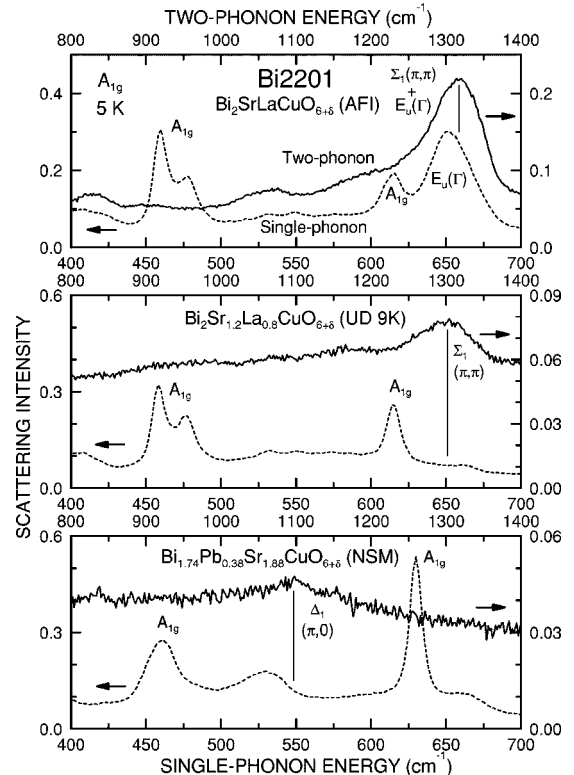
(a) Underdoped Region (b) Optimally doped Region (c) Overdoped Region
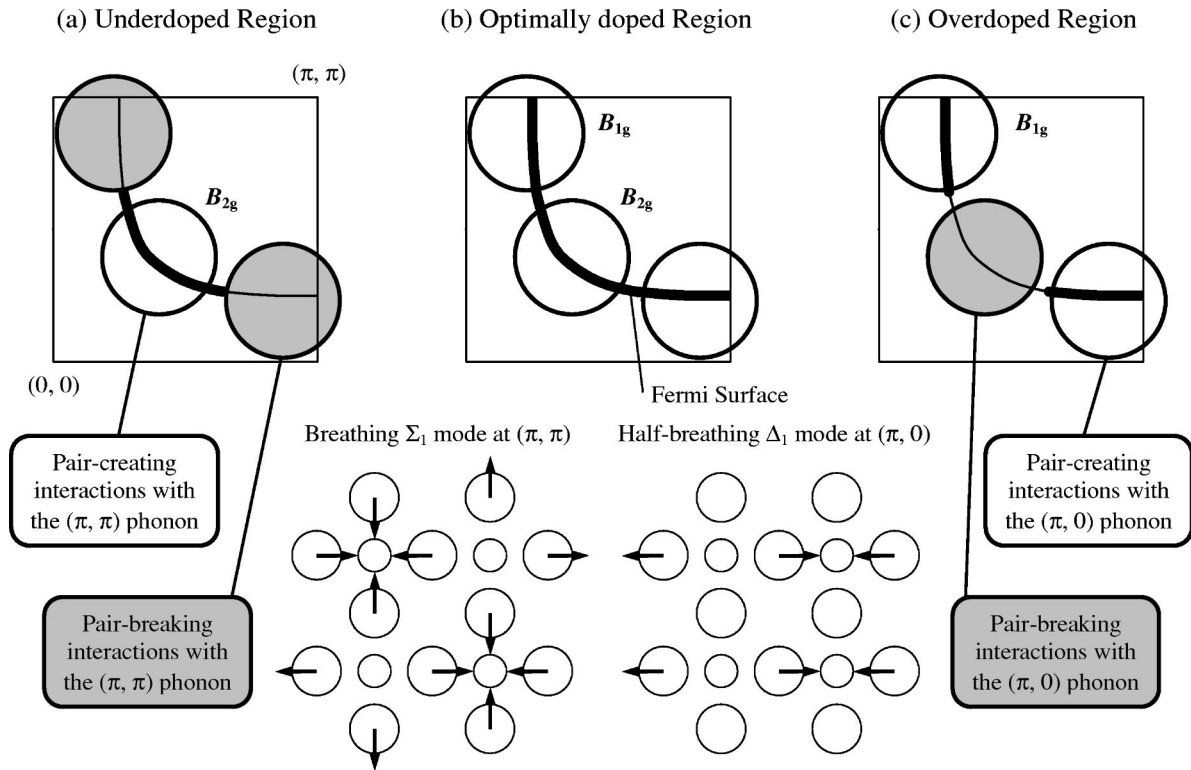
FIG. 23. Schematic diagram for the typical change of electronic states as carrier density increases. The thick curves indicate the Fermi surface with the large electronic density of states above T_c and the thin curves indicate the Fermi surface with the small density of states. The open (gray) circles indicate the areas in which the superconductivity is enhanced (reduced) by the interactions with phonons. The phonon mode with the strongest electron-phonon interaction changes from the breathing Σ_1 mode at (π,π) to the half-breathing Δ_1 mode at $(\pi,0)$ as carrier density increases. The atomic displacement of these modes is illustrated. The small circles are copper atoms and the large circles are oxygen atoms. Electronic excitations around $(\pi/2,\pi/2)$ and $(\pi,0)$ are observed in the B_{2g} and B_{1g} spectra, respectively.

V. CONCLUSIONS

In conclusion the carrier-density-induced momentum change of the superconducting coherent peak from $(\pi/2,\pi/2)$ to $(\pi,0)$ is correlated with the change of the electronic density of states near E_F, but it is not enough to explain the sharp crossover of the coherent peak in YBCO and LSCO. We disclosed that the phonon mode with the strongest electron-phonon interaction changes from the breathing Σ_1 (π,π) mode to the half-breathing Δ_1 $(\pi,0)$ mode on the highest-energy LO branch as carrier density increases. This change is strongly correlated with the change of the coherent peak. It indicates that the superconducting region in k space is limited by the electron-phonon interactions, even if d-wave superconductivity is generated by magnetic interactions. The present experiments support the model by Shen, Lanzara, Ishihara, and Nagaosa where the half-breathing mode modifies the magnetic-interaction-mediated superconductivity.[41]

The suppression of the superconductivity at the maximum gap region near $(\pi,0)$ reduces T_c in the underdoped region, otherwise T_c may increase with the increase of J^* as carrier density decreases. In YBCO the crossover occurs in the 60-K phase, $p=0.1$, and the coherent peak is small at both $(\pi/2,\pi/2)$ and $(\pi,0)$ around this carrier density. The crossover of the coherent peak position in k space induced by electron-phonon interactions is a possible origin for the 60-K phase in YBCO.

[1] J. Mesot, M.R. Norman, H. Ding, M. Randeria, J.C. Campuzano, A. Paramekanti, H.M. Fretwell, A. Kaminski, T. Takeuchi, T. Yokoya, T. Sato, T. Takahashi, T. Mochiku, and K. Kadowaki, Phys. Rev. Lett. **83**, 840 (1999).

[2] D.A. Wollman, D.J. Van Harlingen, W.C. Lee, D.M. Ginsberg, and A.J. Leggett, Phys. Rev. Lett. **71**, 2134 (1993).

[3] C.C. Tsuei, J.R. Kirtley, C.C. Chi, Lock See Yu-Jahnes, A. Gupta, T. Shaw, J.Z. Sun, and M.B. Ketchen, Phys. Rev. Lett. **73**, 593 (1994).

[4] T.P. Devereaux, D. Einzel, B. Stadlober, R. Hackl, D.H. Leach,

and J.J. Neumeier, Phys. Rev. Lett. **72**, 396 (1994).

[5] T.P. Devereaux and D. Einzel, Phys. Rev. B **51**, 16 336 (1995).

[6] S.L. Cooper, M.V. Klein, B.G. Pazol, J.P. Rice, and D.M. Ginsberg, Phys. Rev. B **37**, 5920 (1988).

[7] T. Staufer, R. Nemetschek, R. Hackl, P. Müller, and H. Veith, Phys. Rev. Lett. **68**, 1069 (1992).

[8] X.K. Chen, E. Altendorf, J.C. Irwin, R. Liang, and W.N. Hardy, Phys. Rev. B **48**, 10 530 (1993).

[9] X.K. Chen, J.C. Irwin, H.J. Trodahl, T. Kimura, and K. Kishio, Phys. Rev. Lett. **73**, 3290 (1994).

[10] C. Kendziora and A. Rosenberg, Phys. Rev. B **52**, R9867 (1995).

[11] C. Kendziora, R.J. Kelley, and M. Onellion, Phys. Rev. Lett. **77**, 727 (1996).

[12] X.K. Chen, J.G. Naeini, K.C. Hewitt, J.C. Irwin, R. Liang, and W.N. Hardy, Phys. Rev. B **56**, R513 (1997).

[13] R. Nemetschek, M. Opel, C. Hoffmann, P.F. Müller, R. Hackl, H. Berger, L. Forró, A. Erb, and E. Walker, Phys. Rev. Lett. **78**, 4837 (1997).

[14] J.G. Naeini, X.K. Chen, K.C. Hewitt, J.C. Irwin, T.P. Devereaux, M. Okuya, T. Kimura, and K. Kishio, Phys. Rev. B **57**, R11 077 (1998).

[15] M. Opel, R. Nemetschek, C. Hoffmann, P.F. Müller, R. Philipp, R. Hackl, H. Berger, L. Forró, A. Erb, and E. Walker, J. Phys. Chem. Solids **59**, 1942 (1998).

[16] H.L. Liu, G. Blumberg, M.V. Klein, P. Guptasarma, and D.G. Hinks, Phys. Rev. Lett. **82**, 3524 (1999).

[17] J.G. Naeini, X.K. Chen, J.C. Irwin, M. Okuya, T. Kimura, and K. Kishio, Phys. Rev. B **59**, 9642 (1999).

[18] M. Opel, R. Nemetschek, C. Hoffmann, R. Philipp, P.F. Müller, R. Hackl, I. Tüttő, A. Erb, B. Revaz, E. Walker, H. Berger, and L. Forró, Phys. Rev. B **61**, 9752 (2000).

[19] S. Sugai and T. Hosokawa, Phys. Rev. Lett. **85**, 1112 (2000).

[20] K.C. Hewitt and J.C. Irwin, Phys. Rev. B **66**, 054516 (2002).

[21] K. Kishio, J. Shimoyama, T. Hasegawa, and K. Kitazawa, Jpn. J. Appl. Phys., Part 2 **26**, L1228 (1987).

[22] J.L. Tallon, C. Bernhard, H. Shaked, R.L. Hitterman, and J.D. Jorgensen, Phys. Rev. B **51**, 12 911 (1995).

[23] C.M. Varma, P.B. Littlewood, S. Schmitt-Rink, E. Abrahams, and A.E. Ruckenstein, Phys. Rev. Lett. **63**, 1996 (1989).

[24] T. Valla, A.V. Fedorov, P.D. Johnson, B.O. Wells, S.L. Hulbert, Q. Li, G.D. Gu, and N. Koshizuka, Science **285**, 2110 (1999).

[25] T. Valla, A.V. Fedorov, P.D. Johnson, Q. Li, G.D. Gu, and N. Koshizuka, Phys. Rev. Lett. **85**, 828 (2000).

[26] D.R. Wake, F. Slakey, M.V. Klein, J.P. Rice, and D.M. Ginsberg, Phys. Rev. Lett. **67**, 3728 (1991).

[27] A.G. Panfilov, M.F. Limonov, A.I. Rykov, S. Tajima, and A. Yamanaka, Phys. Rev. B **57**, R5634 (1998).

[28] A.R. Moodenbaugh, Youwen Xu, M. Suenaga, T.J. Folkerts, and R.N. Shelton, Phys. Rev. B **38**, 4596 (1988).

[29] K. Kumagai, Y. Nakamura, I. Watanabe, Y. Nakamichi, and H. Nakajima, J. Magn. Magn. Mater. **76−77**, 601 (1988).

[30] J.M. Tranquada, B.J. Sternlieb, J.D. Axe, Y. Nakamura, and S. Uchida, Nature (London) **375**, 561 (1995).

[31] T. Katsufuji, Y. Tokura, T. Ido, and S. Uchida, Phys. Rev. B **48**, 16 131 (1993).

[32] J.G. Naeini, J.C. Irwin, T. Sasagawa, Y. Togawa, and K. Kishio, Can J. Phys. **78**, 483 (2000).

[33] F. Venturini, M. Opel, T.P. Devereaux, J.K. Freericks, I. Tüttő, B. Revaz, E. Walker, H. Berger, L. Forró, and R. Hackl, Phys. Rev. Lett. **89**, 107003 (2002).

[34] S. Sugai, S. Shamoto, and M. Sato, Phys. Rev. B **38**, 6436 (1988).

[35] G. Blumberg, M. Kang, M.V. Klein, K. Kadowaki, and C. Kendziora, Science **278**, 1427 (1997).

[36] Z.-X. Shen and J.R. Schrieffer, Phys. Rev. Lett. **78**, 1771 (1997).

[37] N. Furukawa, T.M. Rice, and M. Salmhofer, Phys. Rev. Lett. **81**, 3195 (1998).

[38] K. Tsutsui, T. Tohyama, and S. Maekawa, Phys. Rev. Lett. **83**, 3705 (1999).

[39] M.R. Norman, H. Ding, M. Randeria, J.C. Campuzano, T. Yokoya, T. Takeuchi, T. Takahashi, T. Mochiku, K. Kadowaki, P. Guptasarma, and D.G. Hinks, Nature (London) **392**, 157 (1998).

[40] P.V. Bogdanov, A. Lanzara, X.J. Zhou, W.L. Yang, H. Eisaki, Z. Hussain, and Z.X. Shen, Phys. Rev. Lett. **89**, 167002 (2002).

[41] Z.-X. Shen, A. Lanzara, S. Ishihara, and N. Nagaosa, Philos. Mag. B **82**, 1349 (2002).

[42] S. Sugai, Phys. Rev. B **39**, 4306 (1989).

[43] M. Yoshida, S. Tajima, N. Koshizuka, S. Tanaka, S. Uchida, and T. Itoh, Phys. Rev. B **46**, 6505 (1992).

[44] M. Reedyk, C. Thomsen, M. Cardona, J.S. Xue, and J.E. Greedan, Phys. Rev. B **50**, 13 762 (1994).

[45] C.C. Homes, A.W. McConnell, B.P. Clayman, D.A. Bonn, Ruixing Liang, W.N. Hardy, M. Inoue, H. Negishi, P. Fournier, and R.L. Greene, Phys. Rev. Lett. **84**, 5391 (2000).

[46] J.J. Tu, C.C. Homes, G.D. Gu, and M. Strongin, Physica B **316−317**, 324 (2002).

[47] S. Uchida, T. Ido, H. Takagi, T. Arima, Y. Tokura, and S. Tajima, Phys. Rev. B **43**, 7942 (1991).

[48] L. Pintschovius, N. Pyka, W. Reichardt, A.Y. Rumiantsev, N.L. Mitrofanov, A.S. Ivanov, G. Collin, and P. Bourges, Physica C **185−189**, 156 (1991).

[49] S. Tajima, T. Ido, S. Ishibashi, T. Itoh, H. Eisaki, Y. Mizuo, T. Arima, H. Takagi, and S. Uchida, Phys. Rev. B **43**, 10 496 (1991).

[50] M.A. Quijada, D.B. Tanner, F.C. Chou, D.C. Johnston, and S.-W. Cheong, Phys. Rev. B **52**, 15 485 (1995).

[51] H. Rietschel, L. Pintschovius, and W. Reichardt, Physica C **162−164**, 1705 (1989).

[52] R. Henn, A. Wittlin, M. Cardona, and S. Uchida, Phys. Rev. B **56**, 6295 (1997).

[53] R.M. Martin, Phys. Rev. B **4**, 3676 (1971).

[54] E.T. Heyen, J. Kircher, and M. Cardona, Phys. Rev. B **45**, 3037 (1992).

[55] L. Pintschovius and W. Reichardt, in *Physical Properties of High Temperature Superconductors IV*, edited by P. Ginsberg (World Scientific, Singapore, 1995), p. 295.

[56] L. Pintschovius and M. Braden, Phys. Rev. B **60**, 15 039 (1999).

[57] C. Falter, M. Klenner, and W. Ludwig, Phys. Rev. B **47**, 5390 (1993).

[58] C. Falter, M. Klenner, and G.A. Hoffmann, Phys. Rev. B **52**, 3702 (1995).

[59] C. Falter, M. Klenner, G.A. Hoffmann, and Q. Chen, Phys. Rev. B **55**, 3308 (1997).

[60] C. Falter and G.A. Hoffmann, Phys. Rev. B **61**, 14 537 (2000).

[61] C. Falter and F. Schnetgöke, Phys. Rev. B **65**, 054510 (2002).

[62] H.A. Mook and F. Doğan, Nature (London) **401**, 145 (1999).

[63] R.J. McQueeney, Y. Petrov, T. Egami, M. Yethiraj, G. Shirane, and Y. Endoh, Phys. Rev. Lett. **82**, 628 (1999).

[64] R.J. McQueeney, J.L. Sarrao, P.G. Pagliuso, P.W. Stephens, and R. Osborn, Phys. Rev. Lett. **87**, 077001 (2001).

[65] E.T. Heyen, J. Kircher, and M. Cardona, Phys. Rev. B **45**, 3037 (1992).

[66] M. Bauer, I.B. Ferreira, L. Genzel, M. Cardona, P. Murugaraj, and J. Maier, Solid State Commun. **72**, 551 (1989).

[67] M.K. Crawford, G. Burns, and F. Holtzberg, Solid State Commun. **70**, 557 (1989).

[68] H.J. Ye, R.P. McCall, W.E. Farneth, E.M. McCarron, III, and A.J. Epstein, Phys. Rev. B **43**, 10 574 (1991).

[69] J. Schützmann, S. Tajima, S. Miyamoto, Y. Sato, and R. Hauff, Phys. Rev. B **52**, 13 665 (1995).

[70] L. Pintschovius, W. Reichardt, M. Kläser, T. Wolf, and H.v. Löhneysen, Phys. Rev. Lett. **89**, 037001 (2002).

[71] D. Reznik, L. Pintschovius, W. Reichardt, Y. Endoh, H. Hiraka, J.M. Tranquada, S. Tajima, H. Uchiyama, and T. Masui, J. Low Temp. Phys. **131,** 417 (2003).

[72] S. Sugai and M. Sato, Phys. Rev. B **40**, 9292 (1989).

[73] R. Liu, M.V. Klein, P.D. Han, and D.A. Payne, Phys. Rev. B **45**, 7392 (1992).

[74] M. Kakihana, M. Osada, M. Käll, L. Börjesson, H. Mazaki, H. Yasuoka, M. Yashima, and M. Yoshimura, Phys. Rev. B **53**, 11 796 (1996).

[75] B. Renker, F. Gompf, D. Ewert, P. Adelmann, H. Schmidt, E. Gering, and H. Mutka, Z. Phys. B: Condens. Matter **77**, 65 (1989).

[76] S. Tajima, G.D. Gu, S. Miyamoto, A. Odagawa, and N. Koshizuka, Phys. Rev. B **48**, 16 164 (1993).

[77] A.A. Tsvetkov, D. Dulić, D. van der Marel, A. Damascelli, G.A. Kaljushnaia, J.I. Gorina, N.N. Senturina, N.N. Kolesnikov, Z.F. Ren, J.H. Wang, A.A. Menovsky, and T.T.M. Palstra, Phys. Rev. B **60**, 13 196 (1999).

[78] M. Osada, M. Kakihana, M. Käll, L. Börjesson, A. Inoue, and M. Yashima, Phys. Rev. B **56**, 2847 (1997).

[79] A.F. Goncharov, V.V. Struzhkin, E. Gregoryanz, J. Hu, R.J. Hemley, Ho-kwang Mao, G. Lapertot, S.L. Bud'ko, and P.C. Canfield, Phys. Rev. B **64**, 100509 (2001).

[80] J. Hlinka, I. Gregora, J. Pokorný, A. Plecenik, P. Kúš, L. Satrapinsky, and Š. Beňačka, Phys. Rev. B **64**, 140503 (2001).

[81] J.W. Quilty, S. Lee, A. Yamamoto, and S. Tajima, Phys. Rev. Lett. **88**, 087001 (2002).

[82] A. Lanzara, P.V. Bogdanov, X.J. Zhou, S.A. Kellar, D.L. Feng, E.D. Lu, T. Yoshida, H. Eisaki, A. Fujimori, K. Kishio, J.-I. Shimoyama, T. Noda, S. Uchida, Z. Hussain, and Z.-X. Shen, Nature (London) **412**, 510 (2001).

[83] A. Kaminski, J. Mesot, H. Fretwell, J.C. Campuzano, M.R. Norman, M. Randeria, H. Ding, T. Sato, T. Takahashi, T. Mochiku, K. Kadowaki, and H. Hoechst, Phys. Rev. Lett. **84**, 1788 (2000).

[84] T. Valla, A.V. Fedorov, P.D. Johnson, Q. Li, G.D. Gu, and N. Koshizuka, Phys. Rev. Lett. **85**, 828 (2000).

[85] P.V. Bogdanov, A. Lanzara, S.A. Kellar, X.J. Zhou, E.D. Lu, W.J. Zheng, G. Gu, J.-I. Shimoyama, K. Kishio, H. Ikeda, R. Yoshizaki, Z. Hussain, and Z.X. Shen, Phys. Rev. Lett. **85**, 2581 (2000).

[86] A. Kaminski, M. Randeria, J.C. Campuzano, M.R. Norman, H. Fretwell, J. Mesot, T. Sato, T. Takahashi, and K. Kadowaki, Phys. Rev. Lett. **86**, 1070 (2001).